Haemoglobin causes neuronal damage *in vivo* which is preventable by haptoglobin

Patrick Garland[1], Matthew J Morton[1,*], William Haskins[1,*], Ardalan Zolnourian[2], Andrew Durnford[2], Ben Gaastra[2], Jamie Toombs[3,4], Amanda J Heslegrave[3,4], John More[5], Azubuike I Okemefuna[5], Jessica L Teeling[6], Jonas H Graversen[7], Henrik Zetterberg[3,4,8,9], Soren K Moestrup[7,10,11,#], Diederik O Bulters[2,#], Ian Galea[1,2,#,ψ]

* these authors contributed equally

[#] joint senior authors

[ψ] corresponding author: I.Galea@soton.ac.uk

[1] Clinical Neurosciences, Clinical & Experimental Sciences, Faculty of Medicine, University of Southampton, Southampton, United Kingdom

[2] Wessex Neurological Centre, University Hospital Southampton NHS Foundation Trust, Southampton, United Kingdom

[3] UK Dementia Research Institute, University College London, UK

[4] Department of Neurodegenerative disease, Institute of Neurology, London, UK

[5] R&D, Bio Products Laboratory Limited, Elstree, Hertfordshire, United Kingdom

[6] Biological Sciences, Faculty of Environmental and Life Sciences, University of Southampton, Southampton, United Kingdom

[7] Department of Molecular Medicine, University of Southern Denmark, 5000 Odense, Denmark

[8] Department of Psychiatry and Neurochemistry, Institute of Neuroscience and Physiology, The Sahlgrenska Academy at the University of Gothenburg, Mölndal, Sweden

[9] Clinical Neurochemistry Laboratory, Sahlgrenska University Hospital, Mölndal, Sweden

[10] Department of Clinical Biochemistry and Pharmacology, Odense University Hospital, 5000 Odense, Denmark

[11] Department of Biomedicine, Aarhus University, Aarhus, Denmark

Short title: Haptoglobin blocks haemoglobin neurotoxicity

Abstract

After subarachnoid haemorrhage, prolonged exposure to toxic extracellular haemoglobin occurs in the brain. Here we investigate the role of haemoglobin neurotoxicity *in vivo*, and its prevention. In humans after subarachnoid haemorrhage, haemoglobin in cerebrospinal fluid was associated with neurofilament light chain, a marker of neuronal damage. Most haemoglobin was not complexed with haptoglobin, an endogenous haemoglobin scavenger. Exogenously-added haptoglobin bound most uncomplexed haemoglobin, in the first two weeks after human subarachnoid haemorrhage, indicating a wide therapeutic window. In mice, the behavioural, vascular, cellular and molecular changes seen after human subarachnoid haemorrhage were recapitulated by modelling a single aspect of subarachnoid haemorrhage: prolonged intrathecal exposure to haemoglobin. Haemoglobin-induced behavioural deficits and astrocytic, microglial and synaptic changes were attenuated by haptoglobin. Haptoglobin treatment did not attenuate large-vessel vasospasm, yet improved clinical outcome by restricting diffusion of haemoglobin into the parenchyma and reducing small-vessel vasospasm. In summary haemoglobin toxicity is of clinical importance and preventable by haemoglobin, independent of large vessel vasospasm.

Keywords: subarachnoid haemorrhage, haptoglobin, haemoglobin, neurofilament light chain, outcome

Abbreviations:

CI confidence interval

EVD external ventricular drain

GFAP glial fibrillary acidic protein

Hb haemoglobin

Hp haptoglobin

Iba1 ionized calcium binding adapter molecule 1

IQR inter-quartile range

MCA middle cerebral artery

NFL neurofilament light chain

PBS physiological buffered saline

PFA paraformaldehyde

RBC red blood cell

ROX-SE 5-(6)-carboxy-X-rhodamine, succinimidyl ester

SAH subarachnoid haemorrhage

SEM standard error of the mean

UPLC ultra-performance liquid chromatography

WFNS World Federation of Neurological Surgeons

Abbreviated summary (50 words)

Extracellular haemoglobin is toxic; its contribution to neuronal damage *in vivo* was unknown. Garland *et al* show that exposing the brain to haemoglobin recapitulates the clinicopathological features of subarachnoid haemorrhage. These features are preventable by administration of haptoglobin, which keeps haemoglobin out of the brain tissue, limiting neuronal damage.

Introduction

After subarachnoid haemorrhage (SAH), blood is released into the subarachnoid space (Macdonald and Schweizer, 2017). As the blood clot in the subarachnoid space is resorbed, red blood cell (RBC) lysis leads to the release of cell-free haemoglobin (Hb) over a protracted period exerting a further secondary, and thus potentially reversible, injury. There is a sound biological rationale to hypothesize that prolonged exposure to Hb in the subarachnoid compartment impacts long term outcome (Bulters *et al.*, 2018). Outside of the controlled environment of the erythrocyte, Hb and its breakdown products (haem, bilirubin and free iron) are involved in toxic redox reactions via the iron atom (Reeder, 2010, 2017), leading to oxidation of DNA, protein and lipids, and hence cellular dysfunction, and brain injury.

Focal intracortical injection of a high concentration of Hb causes seizures (Rosen and Frumin, 1979). Similar injections of whole blood in the striatum of mice causes neurologic deficits such as posturing, incoordination and/or paresis (Zhao *et al.*, 2009). Less is known about the neurological consequences of prolonged exposure to lower concentrations of Hb distributed throughout the ventricular system, as happens during clot lysis after SAH. Repeated cisterna magna injections of washed autologous red blood cells in rabbits caused iron deposition and a microglial reaction in the cerebellum, but neuronal integrity and behavioural deficits were not studied (Koeppen and Borke, 1991). A single intraventricular Hb injection in 7 day old neonatal rats caused neuronal damage (Garton *et al.*, 2016), so a similar process could occur after prolonged exposure to subarachnoid Hb in adults.

Haptoglobin (Hp) is the body's natural defence against extracellular Hb (Andersen *et al.*, 2017). Hp lowers the redox potential of Hb to prevent damaging peroxidative reactions, and chaperones Hb to prevent haem release and its degradation to free iron. Intrathecal Hp concentration is significantly lower compared to plasma, and most of the Hb after SAH is not bound to Hp (Galea *et al.*, 2012). Therefore, direct supplementation with exogenous Hp, which would be expected to increase CNS Hp concentration more rapidly and to a higher level than drug-induced upregulation of Hp synthesis, might be expected to be of therapeutic benefit after SAH.

This project consists of human, *in vitro* and *in vivo* animal studies, presented in this order. First, we sought to identify whether tissue damage was linked to Hb after SAH in humans. Then, in

experimental models, we tested whether prolonged intrathecal exposure to pure Hb is neurotoxic and causes behavioural abnormalities similar to those seen after human SAH. To model prolonged intrathecal Hb exposure, the mouse ventricular system was infused with a clinically relevant Hb concentration for two weeks. We studied behavioural deficits, large vessel and parenchymal vasospasm, the astrocytic and microglial/macrophage reaction to Hb, and synaptic loss. Finally, we assessed if these changes were reversed by administration of Hp.

Materials and Methods

Human study

Human studies were performed in accordance with the ethical standards as laid down in the 1964 Declaration of Helsinki. 19 control participants were patients with non-inflammatory non-haemorrhagic conditions who underwent lumbar puncture and were subsequently found to have normal CSF (National Research Ethics Committee approval number 11/SC/0204). 44 Fisher grade III-IV non-traumatic SAH patients, requiring an external ventricular drain (EVD) as part of their clinical management (to manage acute hydrocephalus), were recruited (National Research Ethics Committee approval number 12/SC/0666). CSF was obtained from the EVD on alternate days until removal of the EVD. CSF was drawn from a three way tap connecting the ventricular catheter (approximately 30cm long) to the tubing leading to an external CSF drainage and monitoring system (Becker®, Medtronic). For sampling, the tap was opened to the ventricular catheter, and closed to the drainage system. The first 3ml of CSF (representing dead space) was discarded to ensure fresh CSF was obtained. Only 42 patients contributed to this study due to early removal of the EVD. CSF was centrifuged at 1500 rcf for 10 minutes at 21°C and frozen within one hour of sampling.

Ultra-performance liquid chromatography (UPLC) was used to separate CSF components in a tris-saline mobile phase, coupled to absorbance measurement at 415 nm to identify haem-containing species. Full details are in Supplementary Material. Hb was measured in CSF before and after saturating with Hp (Bio Products Laboratory Limited, Elstree, UK) to measure Hp-bindable and Hp-unbindable uncomplexed Hb (Fig. 1). CSF neurofilament light chain (NFL) was measured by enzyme-linked immunosorbent assay (UmanDiagnostics, Umea, Sweden) (Supplementary Material).

In vitro study

Primary hippocampal neurones were cultured according to a modified method from the Ittner lab (Fath et al., 2009; Garland et al., 2012) (Supplementary Material). Cultured neurones were challenged with Hb at day 7 until day 14. Over the seven days, Hb concentration was maintained during media changes. An equimolar-binding ratio of Hp (see Supplementary Material) was added concomitantly for Hp treatment experiments. Hb and Hp preparations, immunocytochemistry for microtubule-associated protein-2 and quantification of viable neurones are detailed in Supplementary Material.

In vivo animal model

Mouse model of prolonged intrathecal Hb exposure

To model prolonged intrathecal Hb exposure, a two-week intracerebroventricular infusion of Hb was used. Locally bred male C57BL/6 mice were housed at 21^{o}C under a 12-hour light/12-hour dark cycle in a conventional animal research facility, and allowed access to food and water *ad libitum*; surgery was performed at 10-12 weeks of age. All procedures were performed under U.K. Home Office licence 30-3057 and all applicable international, national, and/or institutional guidelines for the care and use of animals were followed. Alzet osmotic minipumps (Model 2002, #296, two-week infusion, 0.5µl/hr, Charles River, Harlow, Essex) were loaded with vehicle (0.9% saline), Hb, Hb + Hp, or Hp. Treatment allocation was random. The infusate Hb concentration was 20mg/ml to achieve a clinically relevant CSF Hb concentration of 10µM as detailed in Supplementary Material. The Hp concentration was 14mg/ml to achieve 1:1 Hb to Hp binding stoichiometry, guided by data from empirical determination of Hb to Hp binding ratio (Supplementary Material). The minipump was attached to a 30-gauge ventricular cannula using vinyl tubing (Brain Infusion Kit 3, #8851, Charles River, Harlow, Essex), and primed with test solution according to the manufacturer's instructions. Mice were anaesthetised using a ketamine (Bayer, Reading, UK) and xylazine (Pfizer, Tadworth, Surrey, UK) mixture (100 and 10 mg/kg, respectively). The head was immobilized in a stereotactic frame. Mice body temperature was thermostatically controlled with a rectal probe and a heated pad. An aseptic technique was used. Blunt dissection was used to create a subcutaneous pocket in the interscapular region for insertion of the minipump. A burr hole was drilled and the ventricular cannula inserted at the following coordinates from bregma: anteroposterior, -0.4mm; lateral, 1mm; depth, 2.5mm. Cyanoacrylate was used to secure the cannula holder to the skull surface. Buprenorphine (Centaur, Castle Cary, Somerset, UK) was administered immediately following surgery (0.5mg/kg subcutaneously) and the next

morning in 5ml fruit jelly (300µg/45ml). Mice were housed individually following surgery for 14 days so the experimental unit was a single animal. Mice were checked twice in the first 24 hours and daily thereafter. Residual volume in the minipumps was systematically examined after explantation, at the end of the two weeks, to ensure the appropriate volume of 200µL was delivered while *in situ*. Correct placement of the ventricular cannula was confirmed during tissue sectioning by observing the cannula track.

Behavioural, histological and biochemical readouts

Open-field behavioural analysis was performed in a laser-monitored behaviour arena (Med Associates, Fairfax, VA, US) over a five-minute period, twice a day at the same time in the morning and afternoon, as detailed in Supplementary Material. At 14 days post-surgery, mice were transcardially perfused with heparinised saline (1unit/ml, LEO Pharma, Hurley, Berkshire, UK), followed by 4% paraformaldehyde (PFA) in 0.1M phosphate buffer. Brains were removed and post-fixed in 4% PFA overnight at 4°C and then embedded in paraffin wax. Coronal sections were cut at 10µm, dewaxed in xylene, and rehydrated through graded ethanol/water solutions. Immunohistochemistry and imaging for glial fibrillary acidic protein (GFAP), ionized calcium binding adapter molecule 1 (Iba1), synaptophysin, haemoglobin, CD163 and smooth muscle actin, and Perl's histochemistry was performed as detailed in Supplementary Material. To ensure blinding, all samples were coded prior to image capture and analysis. All analyses were performed by two-dimensional quantification, averaged over two sections per animal within each area studied, and data is presented per mm^2, unless otherwise indicated; further details are in Supplementary Material. For biochemistry, the hemisphere ipsilateral to cannula insertion was homogenised in buffer, after transcardial perfusion with heparinised saline only, and tissue processed for Western blotting as detailed in Supplementary Material.

Fluorescent imaging of Circle of Willis in situ

The method for *in situ* imaging was established in the Zipfel group (Aum *et al.*, 2017). Mice were anaesthetised using a ketamine (Bayer, Reading, UK) and xylazine (Pfizer, Tadworth, Surrey, UK) mixture (100 and 10mg/kg, respectively) and transcardially perfused through the left ventricle with 10mM glucose-PBS followed by 20 mL 20µM 5-(6)-carboxy-X-rhodamine, succinimidyl ester (ROX-SE, Sigma-Aldrich, Gillingham, Dorset, UK) dye in 10mM glucose-PBS prior to perfusions with 4% PFA (in PBS). All perfusions were performed with solutions

at 21°C, at a constant pressure of 80mmHg ±2mmHg using a GE Druck DP1705. Animals were decapitated, the calvaria removed, and post-fixed in 4% PFA in the dark at 4°C for 24 hours. Brains were removed under a dissection microscope to preserve the basal arteries. Then, brains were placed *en bloc* on a glass coverslip and gently covered in PBS before placing on the stage of a confocal laser scanning microscope (SP8, Leica, Wetzlar, Germany). Measurements of anterior and middle cerebral artery (MCA) diameters were made at the narrowest point across the first mm of the vessel, as detailed in Supplementary Material.

Surface plasmon resonance

Surface plasmon resonance analysis was carried out as described (Madsen *et al.*, 2004) using a Biacore 3000 instrument (Biacore, Uppsala, Sweden). Mouse or human CD163, produced using recombinant technology in-house (Kristiansen *et al.*, 2001; Etzerodt *et al.*, 2013), were immobilized in 10mM sodium acetate (pH 4) and remaining binding sites were blocked with 1M ethanolamine (pH 8.5). The resulting densities were: human CD163 0.0468 pmol/mm^2, and murine CD163 0.0320 pmol/mm^2. Sensorgrams were generated using the running buffer CaHBS with 2mM free Ca_2Cl_2 (10mM Hepes, 150mM NaCl, 3.0mM $CaCl_2$, 1.0mM EGTA, + 0.005% P20, and pH 7.4) and the protein concentrations: 5µg/ml of mouse and human Hb (Sigma-Aldrich, Gillingham, Dorset, UK); 7.5 µg/ml of mouse Hp (MyBioSource, San Diego, Ca) and human Hp1-1 (Sigma-Aldrich, Gillingham, Dorset, UK). The flow cell was regenerated in 10mM glycine, 20mM EDTA, 500mM NaCl+0.005% P20, pH4.0 between the runs. All experiments were at least conducted in triplicate and data was evaluated using the BiaEvaluation ver. 4.1 software (Biacore, Uppsala, Sweden).

Statistics

Statistical analysis and graph preparation were performed using SPSS (v24) and GraphPad Prism (v7.01), with data expressed as mean ± standard error of the mean (SEM), median ± interquartile range, or 95% confidence intervals. Normality and heteroscedasticity was routinely determined across all data sets. Where necessary, logarithmic transformation was used to normalise data. α, the probability of a Type I error, was 0.05. Two-tailed hypotheses were considered throughout. Details of individual statistical analyses are available in Supplementary Material. Animals were randomly selected and sequentially assigned to treatment groups. Animal *in vivo* experiments were reported according to ARRIVE guidelines

(Kilkenny *et al.*, 2010), and the checklist is available in Supplementary Material. Supplementary Table 1 summarizes all the analyses performed and the results.

Data availability

Datasets are available from the corresponding author on reasonable request in accordance with the University of Southampton's data-sharing policies, ethical approvals and contracts with the co-authors and their institutions.

Results

Human study

Neurofilament light chain concentration in CSF is predicted by Hb

The ideal test of the hypothesis that exposure of the brain to Hb affects outcome after SAH in humans, is to measure Hb in the CSF serially and relate this to outcome. However this poses a significant practical challenge since it is difficult to sample CSF with sufficient frequency and duration to arrive at a reliable estimate of total Hb exposure over the course of clot lysis, a process taking up to a month (Naff *et al.*, 2001). Therefore we focussed on an initial two-week time interval, during which we serially sampled CSF and investigated whether there was a temporal relationship between Hb and NFL, a marker of neuronal damage (Siedler *et al.*, 2014). We hypothesized that within the two-week sampling window, peak NFL in the CSF could be predicted by the preceding peak Hb. Serial CSF samples were collected from 42 patients with Fisher grade III-IV SAH via an EVD. Control CSF was collected by lumbar puncture in patients with non-inflammatory non-haemorrhagic neurological symptoms. Demographic and clinical characteristics are shown in Table 1. NFL measured by enzyme-linked immunosorbent assay was higher in SAH CSF *versus* control CSF (Fig. 2A). This difference occurred even though there is a ventriculo-lumbar gradient in CSF NFL, with lumbar CSF concentration being higher (Jeppsson *et al.*, 2013). CSF NFL levels after SAH had a wide distribution, some within the reference range (Fig. 2A). CSF samples were analysed using UPLC for Hb species as detected by absorbance in the Soret band at 415nm to quantify total Hb, irrespective of oxidation state (Fig. 1A and B). Total Hb increased gradually from the third day post-ictus onwards, peaking at day 11 (Fig. 2B) and reaching a plateau between days 11 and 13. There was a small initial spike in CSF NFL level, followed by a gradual rise (Fig. 2B). The gradual rise in NFL (day 5 onwards) followed the rise in Hb (day 3 onwards) (Fig. 2B). When comparing patients with high *versus* normal peak CSF NFL levels, the former had significantly

higher CSF Hb levels preceding the peak CSF NFL (Fig. 2C). Peak NFL concentration in serial CSF samples was predicted by the peak Hb level preceding it, controlling for initial neurological state as determined by the World Federation of Neurological Surgeons (WFNS) (Teasdale *et al.*, 1988), age and sex (Fig. 2D).

An opportunistic therapeutic window for intrathecal Hp supplementation after SAH

Hp is present at low levels in CSF (Galea *et al.*, 2012), so we set out to find the percentage of Hb complexed to Hp after SAH. Hb-Hp complexes could be differentiated from uncomplexed Hb, due to the difference in retention time on the column, and a corresponding difference in peak size (Fig. 1B). Most of the Hb was uncomplexed (median 96.3%, IQR: 83.3-99.4%, from third day onwards, Fig. 2E).

The prolonged presence of Hb in a pro-inflammatory acidotic environment is particularly conducive to denaturing modifications of Hb, rendering it less able to bind Hp (Vallelian *et al.*, 2008). Modified Hb forms have been detected in CSF after SAH (Reeder *et al.*, 2002), and their formation has the potential to interfere with the therapeutic potential of Hp. Therefore, we asked whether the uncomplexed Hb in the CSF after SAH could be bound by exogenous Hp. CSF was first run on UPLC on its own. Then exogenous Hp was added in excess of Hb-binding stoichiometry and the mixture run on UPLC to determine the proportion of uncomplexed Hb which could be bound by Hp (Fig. 1C). When exogenous Hp was added to the CSF samples, most of the uncomplexed Hb formed a complex with Hp: 90.6% (IQR: 65.8-96.5%) from the third day onwards (Fig. 2F). Similarly, 76.4% (IQR: 67.7-96.4%) of total uncomplexed Hb could form a complex with Hp during the day 11-13 plateau. Therefore, most uncomplexed Hb in the CSF was available to bind Hp in the first two weeks after ictus. This represents a therapeutic opportunity for intrathecal Hp supplementation after SAH.

In vitro study

Haptoglobin attenuates the toxicity of Hb towards primary mouse neurones

Next, we wanted to confirm that Hp can protect against Hb toxicity. The toxicity of Hb to cortical neurones in mixed glial cultures from foetal mice has been observed previously (Regan and Panter, 1993). We used a protocol that allows culturing of primary hippocampal neurones from mouse pup brain at low density (Fath *et al.*, 2009; Garland *et al.*, 2012) (Fig. 3A).

Microtubule-associated protein 2 (MAP2) positive neurones with 4',6-diamidino-2-phenylindole, dihydrochloride (DAPI)-positive non-apoptotic nuclei (hence viable neurones) were counted following a one-week challenge with increasing concentrations of mouse Hb. The number of viable neurones was found to be reduced after exposure to Hb concentrations above 1μM (Fig. 3A-C). Concomitant addition of an equimolar amount of Hp completely neutralized this Hb toxicity (Fig. 3D).

In vivo animal model

Prolonged intrathecal exposure to Hb causes behavioural deficits, which are attenuated by Hp

A therapeutic potential for Hp has been strongly suggested by experiments in an animal model of focal intraparenchymal cerebral haemorrhage, in which Hp overexpression reversed some of the acute neurological deficits after a large (12μL) intrastriatal injection of whole blood (Zhao *et al.*, 2009). This study provided valuable information, yet the mechanical and inflammatory consequences of a large intraparenchymal injection, and the associated plasma proteins, cell membranes, and white cell constituents, meant that it could not be definitely concluded that Hp targeted the Hb component. Moreover, in the same study Hp expression was manipulated indirectly *in vivo* (Zhao *et al.*, 2009), making it hard to be absolutely certain that Hp was the neuroprotective agent. In order to model the chronic Hb exposure aspect of SAH in isolation, as opposed to the whole SAH condition, adult male C57BL6 mice underwent insertion of an intraventricular cannula attached to a subcutaneously implanted osmotic minipump; this protocol delivered Hb slowly over two weeks (Fig. 4A and B). Male mice were used since (1) sex did not affect Hb neurotoxicity in the human studies (Fig. 2D, n=42, B=0.044 (95% CI:-0.742-0.822), p=0.918), and (2) variability in planned behavioural measures is greater in females, due to the oestrous cycle (Gray and Cooney, 1982). The concentration of Hb was selected to achieve a clinically relevant concentration of 10μM, based on the median total Hb observed in CSF from SAH patients. *In vitro* incubation of Hb or Hb+Hp complexes at 37°C for two weeks showed that Hb did not degrade to release iron, as measured by a free iron assay (Supplementary Fig. 1). The general health of animals in this model was assessed, including daily measurements of weight (Fig. 4C). Perls' staining of brain sections showed iron deposition within the parenchyma and over the convexities (Fig. 4D), the latter confirming circulation of Hb out of the ventricles, into the subarachnoid space, and over the outer surface of the brain.

An automated open-field arena was used to assess mouse ambulatory activity; animals were tested between days 2-13 post-surgery and compared relative to their pre-surgery baseline (Fig. 4E-G). Linear mixed modelling of this time-series data revealed a significant reduction in ambulation in animals challenged with 10μM Hb compared to the vehicle control (Fig. 4F, Supplementary Fig. 2). However, concomitant infusion of Hp with Hb recovered this behavioural deficit (Fig. 4F, Supplementary Fig. 2).

Longer periods of immobility, so-called freezing, in the periphery of the open-field has been described previously as a symptom of anxiety (Simon *et al.*, 1994). Therefore, zonal analysis of the open-field data was performed to measure the time mice spent freezing in the periphery over the first minute (Fig. 4G). A significant increase in freezing was observed in animals challenged with 10μM Hb compared to the vehicle control. This recovered following concomitant treatment with Hp (Fig. 4G).

Prolonged intrathecal exposure to Hb causes a glial reaction and synaptic loss, which are attenuated by Hp

Following behavioural assessment, brain tissue was collected for immunohistochemistry. Two main brain parenchyma regions were selected for quantification (Fig. 5A), close to (cortical region) and distal from (hippocampal region) the infusion site. The microglial/macrophage response to intrathecal Hb was assessed using immunohistochemistry for Iba1, a cytoplasmic protein constitutively expressed by microglia and upregulated during inflammation (Ohsawa *et al.*, 2004). In the cortical region, Iba1-positive cells were more numerous after Hb challenge compared to vehicle challenge (Fig. 5B, C and E). Concomitant infusion of an equimolar-binding amount of Hp with Hb reduced the number of Iba1-positive cells (Fig. 5D and E). A similar Iba1-positive cellular response to Hb was observed caudally, in the glia-rich hippocampal molecular region (Fig. 5F-I) and throughout the hippocampus (Supplementary Fig. 3A).

The astrocytic response to injury from intrathecal Hb was assessed using GFAP. Compared to vehicle, animals challenged with Hb had more GFAP-positive cells in the hippocampal molecular region; this was reversed by concomitant treatment with Hp (Fig. 5J-L). A similar

trend was present throughout the hippocampus (Supplementary Fig. 3B) and cortex (Supplementary Fig. 3C).

We investigated hippocampal synaptic integrity using Sy38, an antibody against the pre-synaptic protein synaptophysin (Fig. 5N-Q). Synaptic loss was observed in Hb animals, relative to vehicle (Fig. 5N, O and Q). Concomitant infusion of Hp with Hb increased Sy38 staining back to control levels (Fig. 5P and Q). A trend towards an interaction between Hb and Hp was found for this marker ($p=0.07$); significant main effects were observed (Supplementary Table 1). A similar picture was observed when tissue was analysed for postsynaptic density protein 95 (psd-95) by western blotting (Supplementary Fig. 4).

CD163 expression

CD163 is the Hb receptor (Kristiansen *et al.*, 2001) and its expression is increased after uptake of Hb (Boyle *et al.*, 2009; Liu *et al.*, 2017). CD163 expression in the brain is very limited (Galea *et al.*, 2012), so it was important to determine whether the Hp therapeutic effect relied on CD163. In order to determine whether the therapeutic effect of Hp was mediated via upregulation of CD163 expression, we used immunohistochemistry. CD163 expression was seen in the meninges and perivascular spaces, as is usual in normal brain (Galea *et al.*, 2008). We did not observe robust changes in CD163 expression after infusion of Hb or Hb-Hp complexes, at either three or 14 days in the parenchyma or convexity (Fig. 6A). Also, surface plasmon resonance demonstrated that human Hp does not increase binding of mouse Hb to mouse CD163 (Fig. 6B), in contrast to the human scavenging system (Fig. 6C). In summary the Hp therapeutic effect did not rely on CD163.

Hp prevents iron deposition

When Hb is oxidised and subsequently degrades, free chelatable iron is released (Asleh *et al.*, 2005; Reeder, 2010). Deposition of this iron in tissue can be visualised using Perls' stain, which we have observed to be increased in post-mortem brain tissue from SAH patients (Garland *et al.*, 2016). Similarly, iron deposition was observed in the parenchyma (Fig. 6D) and on the brain surface and outer layers of the cortex (Fig. 6E) in Hb-challenged animals relative to vehicle. In both locations, Hp treatment reduced iron deposition (Fig. 6D and E). Positive correlations were observed between the Perls' staining and: microglia (Iba1, Supplementary Fig. 5A, B, G and H), astrocytes (GFAP, Supplementary Fig. 5C and I), and freezing

(Supplementary Fig. 5F and L). Negative correlations were observed between the Perls' staining and Sy38 staining in the hippocampus (Supplementary Fig. 5D and J) and ambulation (Supplementary Fig. 5E and K).

Hp prevents diffusion of Hb into the parenchyma and attenuates small-vessel, but not large-vessel, vasospasm

Angiographic large-vessel vasospasm and long-term outcome are dissociated (Diringer, 2013), interventions which attenuate large-vessel vasospasm have proved unsuccessful (Cho *et al.*, 2019) and interventions which improve long-term outcome do not affect large-vessel vasospasm (Pickard *et al.*, 1989). However, dysregulation of microcirculation following SAH is an emerging area of study (Terpolilli *et al.*, 2015). As Hb is a known mediator of vasospasm, we hypothesized that the Hb challenge in our model would promote large and small-vessel vasospasm, and this would be attenuated by Hp. Following a three day infusion of Hb, anaesthetized mice were transcardially perfused with ROX-SE for *in situ* imaging of the Circle of Willis (Fig. 7A, C and F-H). A reduction in middle cerebral artery diameter was observed with Hb *versus* vehicle and this was not reversed by Hp (Fig. 7C). A similar picture (Hb-induced vasospasm, not reversed by Hp) was seen with other cerebral arteries (Supplementary Fig. 6). To study parenchymal microcirculatory changes, the same brains used for large-vessel imaging were then prepared for immunohistochemistry and stained for smooth-muscle actin (SMA; Fig. 7B, D, I and K). The ratio of vessel lumen diameter to wall thickness was used as a metric of vasospasm (Sabri and Macdonald, 2012) (Fig. 7B). Hb caused vasospasm which was reversed by Hp. Two-way ANOVA revealed a significant interaction between Hb and Hp (Fig. 7D). Post-hoc analysis revealed significant vasospasm of SMA+ vessels with Hb compared to vehicle, and a significant recovery with Hp (Fig. 7D and I-K).

Hb may cause vasospasm via decreasing nitric oxide (Kanamaru *et al.*, 1987; Lin *et al.*, 2001), yet Hb-Hp complexes bind nitric oxide with similar affinity to Hb alone (Azarov *et al.*, 2008). After Hb infusion, vasospasm occurred in both large and parenchymal vessels but Hp only reversed vasospasm in parenchymal vessels. Hence it was possible that Hp was influencing the distribution of Hb in the brain. Complexation by Hp, especially the polymeric form, results in sequestration of Hb in moieties with a molecular weight of up to 1760kDa, which would severely restrict entry of Hb into the brain tissue. The movement of solutes into the brain is size-selective; single-domain antibody (17kDa) penetrates brain tissue better than whole

immunoglobulin G (150kDa) (Pizzo *et al.*, 2018), and movement of ovalbumin-immunoglobulin G immune complexes (500-2000kDa (Mosconi *et al.*, 2010)) within brain tissue is significantly limited (Carare *et al.*, 2013). To test the hypothesis that Hp was sequestering Hb outside brain tissue, we assessed the Hb content of the brain parenchyma using immunohistochemistry. At three days post-surgery, the same time point as the observed microcirculatory vasospasm, Hb staining in the ipsilateral parenchyma was significantly increased after Hb infusion, compared to vehicle. Hp reversed this parenchymal increase in Hb content (Fig. 7E).

Discussion

SAH results in the prolonged presence of Hb in the subarachnoid space. In humans after SAH, we followed the course of Hb and a neuronal damage marker over an initial discrete observation window. NFL level in the CSF rose gradually, indicating a prolonged stimulus, as opposed to an acute rise immediately after ictus. CSF Hb concentration was low in the first two days, but subsequently increased to a plateau after ten days, likely due to the cumulative effect of RBC lysis. CSF NFL level followed this rise in Hb with a lag of two days. CSF NFL and preceding Hb peaks were significantly related. NFL was used as a marker for Hb-induced tissue damage, hence the mechanisms underlying NFL release after exposure to Hb were not investigated here; these may include direct neuronal damage or secondary consequences such as inflammation.

While it is well known that SAH results in the prolonged presence of Hb in the subarachnoid space, the pathophysiological consequences of prolonged *in vivo* exposure to Hb have not been investigated in isolation. We confirmed previous observations that Hb is toxic to cultured neurones at clinically relevant concentrations (Regan and Panter, 1993; Zhao *et al.*, 2009). In order to establish a clinically relevant model of prolonged Hb exposure, one needs to consider that SAH survivors experience cognitive, behavioural and emotional deficits (Al-Khindi *et al.*, 2010). Modelling these functional outcomes in pre-clinical research is important (Turan *et al.*, 2017). In both the endovascular perforation and blood injection models of SAH, the open-field paradigm has shown significant changes in ambulation and anxiety (Boyko *et al.*, 2013; Fanizzi *et al.*, 2017). However, it was not known whether prolonged exposure to Hb alone – without the mechanical and ischaemic tissue injury, and potential effects of other blood constituents – could independently contribute to, or suffice for, the occurrence of these behavioural deficits. In this study, we have shown that a two-week intrathecal exposure to Hb does in fact lead to

behavioural deficits similar to those seen in clinic, evidenced by reduced ambulation and increased anxiety. A loss of synaptic integrity, as suggested by immunohistochemistry for synaptophysin, accompanied these behavioural deficits. In response to Hb exposure, accumulation of macrophages/microglia was observed in this model, as happens after human and experimental SAH (Schneider *et al.*, 2015). The increase in GFAP-positive cells seen here parallels the high levels of astrocyte-derived serum GFAP and S100β after human SAH, especially observed in patients with poor outcome (Vos *et al.*, 2006; Lai and Du, 2016). Vasospasm was observed in both large cerebral arteries and arterioles in the parenchyma, as seen in human SAH (Terpolilli *et al.*, 2015; Macdonald and Schweizer, 2017). In summary, we observed behavioural, vascular, cellular and molecular changes strikingly similar to those after SAH, by purely modelling one single aspect of SAH: the prolonged intrathecal exposure to uncomplexed Hb.

This study provides robust and conclusive evidence that uncomplexed Hb is a promising therapeutic target in haemorrhagic brain conditions. Hp can reverse Hb toxicity (Zhao *et al.*, 2009), yet Hp concentration is very low in the brain (Galea *et al.*, 2012). We found that most Hb present in human CSF after SAH was uncomplexed. Most of this uncomplexed Hb retained the capacity to bind exogenously added Hp throughout the first two weeks. Therefore, there is a wide therapeutic window for treatments based on administering or upregulating Hp in the CNS after SAH. In an *in vivo* model, Hp supplementation was well tolerated and reversed the neurological deficit occurring in response to Hb. In addition, Hp reduced the microglial and astrocytic reaction to Hb, and synaptic loss.

We did not observe robust changes in CD163 expression accompanying the therapeutic effect of Hp in this model. In mouse, Hp is not required for binding of Hb to CD163 (Etzerodt *et al.*, 2013), unlike in humans, where the Hb-Hp complex has a ten-fold higher affinity to the scavenging receptor CD163 relative to Hb alone (Kristiansen *et al.*, 2001). Human Hp employed in these experiments did not increase the affinity of mouse Hb to mouse CD163. Taken together these findings suggests that the therapeutic effect of Hp was not mediated by increased Hb uptake. Instead Hp stabilized Hb, preventing its degradation and subsequent release of iron. Iron deposition correlated with behavioural deficits, immunohistochemical markers of an astrocytic and microglial reaction, and synaptic loss. Hence, clinically-relevant Hp protection can be achieved solely by stabilizing Hb in solution, independent of clearance

by CD163. This is particularly encouraging since there is evidence that CD163 binding sites in the human brain are much reduced when compared to the periphery, and fully saturated after SAH (Galea *et al.*, 2012), such that Hb-Hp complexes queue for clearance. Endogenous clearance of CSF into the bloodstream and extracerebral lymphatics occurs via arachnoid granulations, cribriform plate and cranial/spinal nerve roots (Kida *et al.*, 1993; Aspelund *et al.*, 2015). The results in this study confirm that there is therapeutic potential for Hp supplementation despite saturation of CD163 binding sites after SAH.

Hp treatment reduced parenchymal Hb staining, suggesting that another mechanism of action of Hp is to reduce the bioavailability of Hb by sequestering it in large complexes in the subarachnoid space and therefore limiting its diffusion into brain tissue. Hp treatment did not attenuate large-vessel vasospasm, yet improved clinical outcome. Instead, Hp attenuated small-vessel vasospasm. Hence we experimentally confirm that clinical outcome can be improved independently of large vessel vasospasm, in keeping with the clinically-observed dissociation between clinical outcome and angiographic vasospasm.

Haem released by Hb degradation is bound by haemopexin, and the complex is cleared by CD91 receptor-mediated endocytosis (Hvidberg *et al.*, 2005), providing a natural defence mechanism against haem. Both haemopexin and CD91 are expressed by neurones and glia (Moestrup *et al.*, 1992; Morris *et al.*, 1993). Haemopexin, in contrast to Hp, has a much higher concentration in CSF than anticipated from its plasma concentration (Garland *et al.*, 2016). This suggests that haemopexin may mediate protection from haem. However a higher CSF haemopexin level was associated with a worse outcome after SAH (Garland *et al.*, 2016), and it has been shown *in vitro* that haemopexin increases the neurotoxicity of Hb when Hp is absent (Chen-Roetling *et al.*, 2018). It may be possible to improve the therapeutic efficacy of Hp by co-administration with haemopexin.

Future work is needed to determine whether Hp can produce a clinically relevant improvement after SAH, in animal models that recapitulate more features of the condition, such as prechiasmatic blood injection (Sabri *et al.*, 2009), cisternal blood injection or endovascular perforation models (Marbacher *et al.*, 2010). Ideally this modelling is performed in a CD163-humanized mouse model, in view of the marked differences in CD163 biology between mouse and man (Etzerodt *et al.*, 2010; Etzerodt *et al.*, 2013), prior to early phase clinical trials in humans. Another suitable animal model would be the pig, in which Hp increases the affinity

of Hb to CD163, as in the human system (personal communication, JHG and SKM). It is important to ensure that Hp administration is safe in the context of a humanized system since it has been suggested that Hp increases the vulnerability of murine CD163-expressing neurones to Hb (Chen-Roetling and Regan, 2016). In a mouse model of intracerebral haemorrhage, CD163 appeared to be detrimental in the first four days after the bleed, but then conferred protection after four days (Leclerc *et al.*, 2018). This inflection may represent a change in the ratio of CD163 expression by neurones *versus* glia/macrophages (Jing *et al.*, 2018), since myelomonocytic ingress into the CNS is delayed by a few days after an inflammatory stimulus (Andersson *et al.*, 1992).

There are several possible Hp-based therapeutic approaches. Direct intrathecal delivery of Hp after high grade SAH would be feasible by the time Hb starts rising in the CSF, since by then patients are usually in a tertiary neurological centre, and likely to have an EVD *in situ*. Hence Hp and Hb would also be present at the same time in the human situation, as modelled with the osmotic minipump here. The challenge in the human situation relates to ensuring that Hp and Hb are present in the same place, i.e. that intrathecal Hp dosing is such that it reaches the far corners of the subarachnoid space, to ensure that Hb is bound by Hp as soon as it is released. The mouse is not the right species to model the intricacies of Hp dosing in humans in view of different subarachnoid space anatomy, CSF turnover rate and drainage pathways. High purity clinical grade Hp is available, though all preparations available at the moment are a mixture of dimeric and polymeric Hp. In these experiments we used a similar preparation, though it was enriched in dimeric Hp. Future work needs to address the issue of which Hp isoform is most efficacious, especially in view of reported differences in clinical outcome between SAH patients with different *HP* genotypes (Gaastra *et al.*, 2019). It may be preferable to determine an individual's Hp genotype and administer the same Hp type, to prevent unwanted immunological rejection in a brain compartment (the subarachnoid space) which is not immunologically privileged (Galea *et al.*, 2007). Spectrophotometric Hb assays which can be easily adapted to achieve a quantitative measure of Hb concentration (Duiser *et al.*, 2001) are clinically available in most hospitals, and using serial CSF Hb assays, it may be possible to alter the Hp dose on a patient-to-patient and day-to-day basis, to deliver the right amount of Hp at the right time. Our observations that Hp-Hb binding is sufficient for therapeutic efficacy, independent of CD163 or brain penetration, suggest that an alternating intrathecal Hp infusion and CSF drainage protocol may be appropriate. Other possible therapeutic avenues are drugs

which upregulate Hp production such as nuclear factor-erythroid 2 (NF-E2)-related factor 2 (nrf2) inducers (Zolnourian *et al.*, 2019).

In summary, this study provides several novel lines of insight into SAH pathophysiology. In CSF, the time course of NFL, a tissue damage marker followed that of Hb. We confirm experimentally that Hb on its own is sufficient to produce an array of behavioural, vascular, cellular and molecular changes strikingly similar to those after human SAH. Robust evidence is presented here that Hp protects against Hb toxicity *in vivo*, mediated via stabilization of Hb and reduction in iron deposition, and by preventing the entry of Hb into brain tissue. We confirm experimentally the clinically-observed dissociation between angiographic vasospasm and clinical outcome, for the first time in favour of an effective treatment. As treatment options are limited for SAH, further preclinical and clinical work is warranted to establish Hp as a therapy. The observations regarding haptogobin efficacy and mechanism of action may apply to other haemorrhagic conditions.

Acknowledgements

For help with this work, we thank Sarah Kingsland, Richard Chester and Joan Dalton (Bio Products Laboratory Limited); Scott Harris (University of Southampton); Diane Aum, Ananth Vellimana and Gregory Zipfel (Washington University School of Medicine)

Funding

We thank the Medical Research Council, Engineering and Physical Sciences Research Council, Bio Products Laboratory Limited, Smile for Wessex, Royal College of Surgeons of Edinburgh, University of Southampton, The Novo Nordisk Foundation and the Independent Research Foundation Denmark. HZ is a Wallenberg Academy Fellow supported by grants from the UK Dementia Research Institute at UCL and the Swedish and European Research Councils.

Competing interests

AIO is a former employee, and JM is a current employee of Bio Products Laboratory Limited, a plasma-derived therapeutics manufacturing company.

References

Al-Khindi T, Macdonald RL, Schweizer TA. Cognitive and functional outcome after aneurysmal subarachnoid hemorrhage. Stroke 2010; 41(8): e519-36.

Andersen CBF, Stodkilde K, Saederup KL, Kuhlee A, Raunser S, Graversen JH, *et al.* Haptoglobin. Antioxidants & redox signaling 2017; 26(14): 814-31.

Andersson PB, Perry VH, Gordon S. The acute inflammatory response to lipopolysaccharide in CNS parenchyma differs from that in other body tissues. Neuroscience 1992; 48(1): 169-86.

Asleh R, Guetta J, Kalet-Litman S, Miller-Lotan R, Levy AP. Haptoglobin genotype- and diabetes-dependent differences in iron-mediated oxidative stress in vitro and in vivo. Circ Res 2005; 96(4): 435-41.

Aspelund A, Antila S, Proulx ST, Karlsen TV, Karaman S, Detmar M, *et al.* A dural lymphatic vascular system that drains brain interstitial fluid and macromolecules. J Exp Med 2015; 212(7): 991-9.

Aum DJ, Vellimana AK, Singh I, Milner E, Nelson JW, Han BH, *et al.* A novel fluorescent imaging technique for assessment of cerebral vasospasm after experimental subarachnoid hemorrhage. Sci Rep 2017; 7(1): 9126.

Azarov I, He X, Jeffers A, Basu S, Ucer B, Hantgan RR, *et al.* Rate of nitric oxide scavenging by hemoglobin bound to haptoglobin. Nitric Oxide 2008; 18(4): 296-302.

Boyko M, Azab AN, Kuts R, Gruenbaum BF, Gruenbaum SE, Melamed I, *et al.* The neuro-behavioral profile in rats after subarachnoid hemorrhage. Brain Res 2013; 1491: 109-16.

Boyle JJ, Harrington HA, Piper E, Elderfield K, Stark J, Landis RC, *et al.* Coronary intraplaque hemorrhage evokes a novel atheroprotective macrophage phenotype. Am J Pathol 2009; 174(3): 1097-108.

Bulters D, Gaastra B, Zolnourian A, Alexander S, Ren D, Blackburn SL, *et al.* Haemoglobin scavenging in intracranial bleeding: biology and clinical implications. Nat Rev Neurol 2018; 14(7): 416-32.

Carare RO, Teeling JL, Hawkes CA, Puntener U, Weller RO, Nicoll JA, *et al.* Immune complex formation impairs the elimination of solutes from the brain: implications for immunotherapy in Alzheimer's disease. Acta Neuropathol Commun 2013; 1: 48.

Chen-Roetling J, Ma SK, Cao Y, Shah A, Regan RF. Hemopexin increases the neurotoxicity of hemoglobin when haptoglobin is absent. J Neurochem 2018; 145(6): 464-73.

Chen-Roetling J, Regan RF. Haptoglobin increases the vulnerability of CD163-expressing neurons to hemoglobin. J Neurochem 2016; 139(4): 586-95.

Cho SS, Kim SE, Kim HC, Kim WJ, Jeon JP. Clazosentan for Aneurysmal Subarachnoid Hemorrhage: An Updated Meta-Analysis with Trial Sequential Analysis. World Neurosurg 2019; 123: 418-24 e3.

Diringer MN. Controversy: does prevention of vasospasm in subarachnoid hemorrhage improve clinical outcome? Stroke 2013; 44(6 Suppl 1): S29-30.

Duiser HJ, Roelandse FW, Lentjes EG, van Loon J, Souverijn JH, Sturk A. Iterative model for the calculation of oxyhemoglobin, methemoglobin, and bilirubin in absorbance spectra of cerebrospinal fluid. Clin Chem 2001; 47(2): 338-41.

Etzerodt A, Kjolby M, Nielsen MJ, Maniecki M, Svendsen P, Moestrup SK. Plasma clearance of hemoglobin and haptoglobin in mice and effect of CD163 gene targeting disruption. Antioxidants & redox signaling 2013; 18(17): 2254-63.

Etzerodt A, Maniecki MB, Moller K, Moller HJ, Moestrup SK. Tumor necrosis factor alpha-converting enzyme (TACE/ADAM17) mediates ectodomain shedding of the scavenger receptor CD163. J Leukoc Biol 2010; 88(6): 1201-5.

Fanizzi C, Sauerbeck AD, Gangolli M, Zipfel GJ, Brody DL, Kummer TT. Minimal Long-Term Neurobehavioral Impairments after Endovascular Perforation Subarachnoid Hemorrhage in Mice. Sci Rep 2017; 7(1): 7569.

Fath T, Ke YD, Gunning P, Gotz J, Ittner LM. Primary support cultures of hippocampal and substantia nigra neurons. Nat Protoc 2009; 4(1): 78-85.

Gaastra B, Ren D, Alexander S, Bennett ER, Bielawski DM, Blackburn SL, *et al.* Haptoglobin genotype and aneurysmal subarachnoid hemorrhage: Individual patient data analysis. Neurology 2019; 92(18): e2150-e64.

Galea I, Bechmann I, Perry VH. What is immune privilege (not)? Trends Immunol 2007; 28(1): 12-8.

Galea I, Felton LM, Waters S, van Rooijen N, Perry VH, Newman TA. Immune-to-brain signalling: the role of cerebral CD163-positive macrophages. Neurosci Lett 2008; 448(1): 41-6.

Galea J, Cruickshank G, Teeling JL, Boche D, Garland P, Perry VH, *et al.* The intrathecal CD163-haptoglobin-hemoglobin scavenging system in subarachnoid hemorrhage. J Neurochem 2012; 121(5): 785-92.

Garland P, Broom LJ, Quraishe S, Dalton PD, Skipp P, Newman TA, *et al.* Soluble axoplasm enriched from injured CNS axons reveals the early modulation of the actin cytoskeleton. PLoS One 2012; 7(10): e47552.

Garland P, Durnford AJ, Okemefuna AI, Dunbar J, Nicoll JA, Galea J, *et al.* Heme-Hemopexin Scavenging Is Active in the Brain and Associates With Outcome After Subarachnoid Hemorrhage. Stroke 2016; 47(3): 872-6.

Garton TP, He Y, Garton HJ, Keep RF, Xi G, Strahle JM. Hemoglobin-induced neuronal degeneration in the hippocampus after neonatal intraventricular hemorrhage. Brain Res 2016; 1635: 86-94.

Gray P, Cooney J. Stress-induced responses and open-field behavior in estrous and nonestrous mice. Physiol Behav 1982; 29(2): 287-92.

Hvidberg V, Maniecki MB, Jacobsen C, Hojrup P, Moller HJ, Moestrup SK. Identification of the receptor scavenging hemopexin-heme complexes. Blood 2005; 106(7): 2572-9.

Jeppsson A, Zetterberg H, Blennow K, Wikkelso C. Idiopathic normal-pressure hydrocephalus: pathophysiology and diagnosis by CSF biomarkers. Neurology 2013; 80(15): 1385-92.

Jing C, Zhang H, Shishido H, Keep RF, Hua Y. Association of Brain CD163 Expression and Brain Injury/Hydrocephalus Development in a Rat Model of Subarachnoid Hemorrhage. Front Neurosci 2018; 12(313): 313.

Kanamaru K, Waga S, Kojima T, Fujimoto K, Niwa S. Endothelium-dependent relaxation of canine basilar arteries. Part 2: Inhibition by hemoglobin and cerebrospinal fluid from patients with aneurysmal subarachnoid hemorrhage. Stroke 1987; 18(5): 938-43.

Kida S, Pantazis A, Weller RO. CSF drains directly from the subarachnoid space into nasal lymphatics in the rat. Anatomy, histology and immunological significance. Neuropathol Appl Neurobiol 1993; 19(6): 480-8.

Kilkenny C, Browne WJ, Cuthill IC, Emerson M, Altman DG. Improving bioscience research reporting: the ARRIVE guidelines for reporting animal research. PLoS Biol 2010; 8(6): e1000412.

Koeppen AH, Borke RC. Experimental superficial siderosis of the central nervous system. I. Morphological observations. J Neuropathol Exp Neurol 1991; 50(5): 579-94.

Kristiansen M, Graversen JH, Jacobsen C, Sonne O, Hoffman HJ, Law SK, *et al.* Identification of the haemoglobin scavenger receptor. Nature 2001; 409(6817): 198-201.

Lai PM, Du R. Association between S100B Levels and Long-Term Outcome after Aneurysmal Subarachnoid Hemorrhage: Systematic Review and Pooled Analysis. PLoS One 2016; 11(3): e0151853.

Leclerc JL, Lampert AS, Loyola Amador C, Schlakman B, Vasilopoulos T, Svendsen P, *et al.* The absence of the CD163 receptor has distinct temporal influences on intracerebral hemorrhage outcomes. J Cereb Blood Flow Metab 2018; 38(2): 262-73.

Lin G, Macdonald RL, Marton LS, Kowalczuk A, Solenski NJ, Weir BK. Hemoglobin increases endothelin-1 in endothelial cells by decreasing nitric oxide. Biochem Biophys Res Commun 2001; 280(3): 824-30.

Liu R, Cao S, Hua Y, Keep RF, Huang Y, Xi G. CD163 Expression in Neurons After Experimental Intracerebral Hemorrhage. Stroke 2017; 48(5): 1369-75.

Macdonald RL, Schweizer TA. Spontaneous subarachnoid haemorrhage. Lancet 2017; 389(10069): 655-66.

Madsen M, Moller HJ, Nielsen MJ, Jacobsen C, Graversen JH, van den Berg T, *et al.* Molecular characterization of the haptoglobin.hemoglobin receptor CD163. Ligand binding properties of the scavenger receptor cysteine-rich domain region. The Journal of biological chemistry 2004; 279(49): 51561-7.

Marbacher S, Fandino J, Kitchen ND. Standard intracranial in vivo animal models of delayed cerebral vasospasm. Br J Neurosurg 2010; 24(4): 415-34.

Moestrup SK, Gliemann J, Pallesen G. Distribution of the alpha 2-macroglobulin receptor/low density lipoprotein receptor-related protein in human tissues. Cell Tissue Res 1992; 269(3): 375-82.

Morris CM, Candy JM, Edwardson JA, Bloxham CA, Smith A. Evidence for the localization of haemopexin immunoreactivity in neurones in the human brain. Neurosci Lett 1993; 149(2): 141-4.

Mosconi E, Rekima A, Seitz-Polski B, Kanda A, Fleury S, Tissandie E, *et al.* Breast milk immune complexes are potent inducers of oral tolerance in neonates and prevent asthma development. Mucosal Immunol 2010; 3(5): 461-74.

Naff NJ, Williams MA, Rigamonti D, Keyl PM, Hanley DF. Blood clot resolution in human cerebrospinal fluid: evidence of first-order kinetics. Neurosurgery 2001; 49(3): 614-9; discussion 9-21.

Ohsawa K, Imai Y, Sasaki Y, Kohsaka S. Microglia/macrophage-specific protein Iba1 binds to fimbrin and enhances its actin-bundling activity. J Neurochem 2004; 88(4): 844-56.

Pickard JD, Murray GD, Illingworth R, Shaw MD, Teasdale GM, Foy PM, *et al.* Effect of oral nimodipine on cerebral infarction and outcome after subarachnoid haemorrhage: British aneurysm nimodipine trial. BMJ 1989; 298(6674): 636-42.

Pizzo ME, Wolak DJ, Kumar NN, Brunette E, Brunnquell CL, Hannocks MJ, *et al.* Intrathecal antibody distribution in the rat brain: surface diffusion, perivascular transport and osmotic enhancement of delivery. J Physiol 2018; 596(3): 445-75.

Reeder BJ. The redox activity of hemoglobins: from physiologic functions to pathologic mechanisms. Antioxidants & redox signaling 2010; 13(7): 1087-123.

Reeder BJ. Redox and Peroxidase Activities of the Hemoglobin Superfamily: Relevance to Health and Disease. Antioxidants & redox signaling 2017; 26(14): 763-76.

Reeder BJ, Sharpe MA, Kay AD, Kerr M, Moore K, Wilson MT. Toxicity of myoglobin and haemoglobin: oxidative stress in patients with rhabdomyolysis and subarachnoid haemorrhage. Biochem Soc Trans 2002; 30(4): 745-8.

Regan RF, Panter SS. Neurotoxicity of hemoglobin in cortical cell culture. Neurosci Lett 1993; 153(2): 219-22.

Rosen AD, Frumin NV. Focal epileptogenesis after intracortical hemoglobin injection. Exp Neurol 1979; 66(2): 277-84.

Sabri M, Jeon H, Ai J, Tariq A, Shang X, Chen G, *et al.* Anterior circulation mouse model of subarachnoid hemorrhage. Brain Res 2009; 1295: 179-85.

Sabri M, Macdonald RL. Vasospasm: Measurement of Diameter, Perimeter, and Wall Thickness. In: Chen J, Xu X-M, Xu ZC, Zhang JH, editors. Animal Models of Acute Neurological Injuries II: Injury and Mechanistic Assessments, Volume 1. Totowa, NJ: Humana Press; 2012. p. 473-9.

Schneider UC, Davids AM, Brandenburg S, Muller A, Elke A, Magrini S, *et al.* Microglia inflict delayed brain injury after subarachnoid hemorrhage. Acta Neuropathol 2015; 130(2): 215-31.

Siedler DG, Chuah MI, Kirkcaldie MT, Vickers JC, King AE. Diffuse axonal injury in brain trauma: insights from alterations in neurofilaments. Front Cell Neurosci 2014; 8: 429.

Simon P, Dupuis R, Costentin J. Thigmotaxis as an index of anxiety in mice. Influence of dopaminergic transmissions. Behav Brain Res 1994; 61(1): 59-64.

Teasdale GM, Drake CG, Hunt W, Kassell N, Sano K, Pertuiset B, *et al.* A universal subarachnoid hemorrhage scale: report of a committee of the World Federation of Neurosurgical Societies. J Neurol Neurosurg Psychiatry 1988; 51(11): 1457.

Terpolilli NA, Brem C, Buhler D, Plesnila N. Are We Barking Up the Wrong Vessels? Cerebral Microcirculation After Subarachnoid Hemorrhage. Stroke 2015; 46(10): 3014-9.

Turan N, Miller BA, Heider RA, Nadeem M, Sayeed I, Stein DG, *et al.* Neurobehavioral testing in subarachnoid hemorrhage: A review of methods and current findings in rodents. J Cereb Blood Flow Metab 2017; 37(11): 3461-74.

Vallelian F, Pimenova T, Pereira CP, Abraham B, Mikolajczyk MG, Schoedon G, *et al.* The reaction of hydrogen peroxide with hemoglobin induces extensive alpha-globin crosslinking and impairs the interaction of hemoglobin with endogenous scavenger pathways. Free Radic Biol Med 2008; 45(8): 1150-8.

Vos PE, van Gils M, Beems T, Zimmerman C, Verbeek MM. Increased GFAP and S100beta but not NSE serum levels after subarachnoid haemorrhage are associated with clinical severity. Eur J Neurol 2006; 13(6): 632-8.

Zhao X, Song S, Sun G, Strong R, Zhang J, Grotta JC, *et al.* Neuroprotective role of haptoglobin after intracerebral hemorrhage. J Neurosci 2009; 29(50): 15819-27.

Zolnourian A, Galea I, Bulters D. Neuroprotective Role of the Nrf2 Pathway in Subarachnoid Haemorrhage and Its Therapeutic Potential. Oxid Med Cell Longev 2019; 2019: 6218239.

Figure 1. Human study: methodology

Assay of Hb binding by Hp. **a**, UPLC method. CSF alone, or CSF incubated with excess Hp, was run through a C18 column to achieve separation of proteins. The absorbance of the eluate was measured at 415 nm to detect haem-containing species. **b**, A representative CSF chromatogram demonstrating peaks of Hb complexed to dimeric and polymeric Hp, haem complexed to haemopexin and albumin, and uncomplexed Hb. Peak area-under-the-curve was quantified using a Hb standard curve. **c**, Uncomplexed Hb able to bind Hp was measured by running CSF alone (orange), and separately CSF to which excess Hp was added (grey). The increase in complexed Hb peak area after adding excess Hp represents uncomplexed Hb that can bind Hp. The uncomplexed Hb peak remaining after adding excess Hp represents uncomplexed Hb unable to bind Hp.

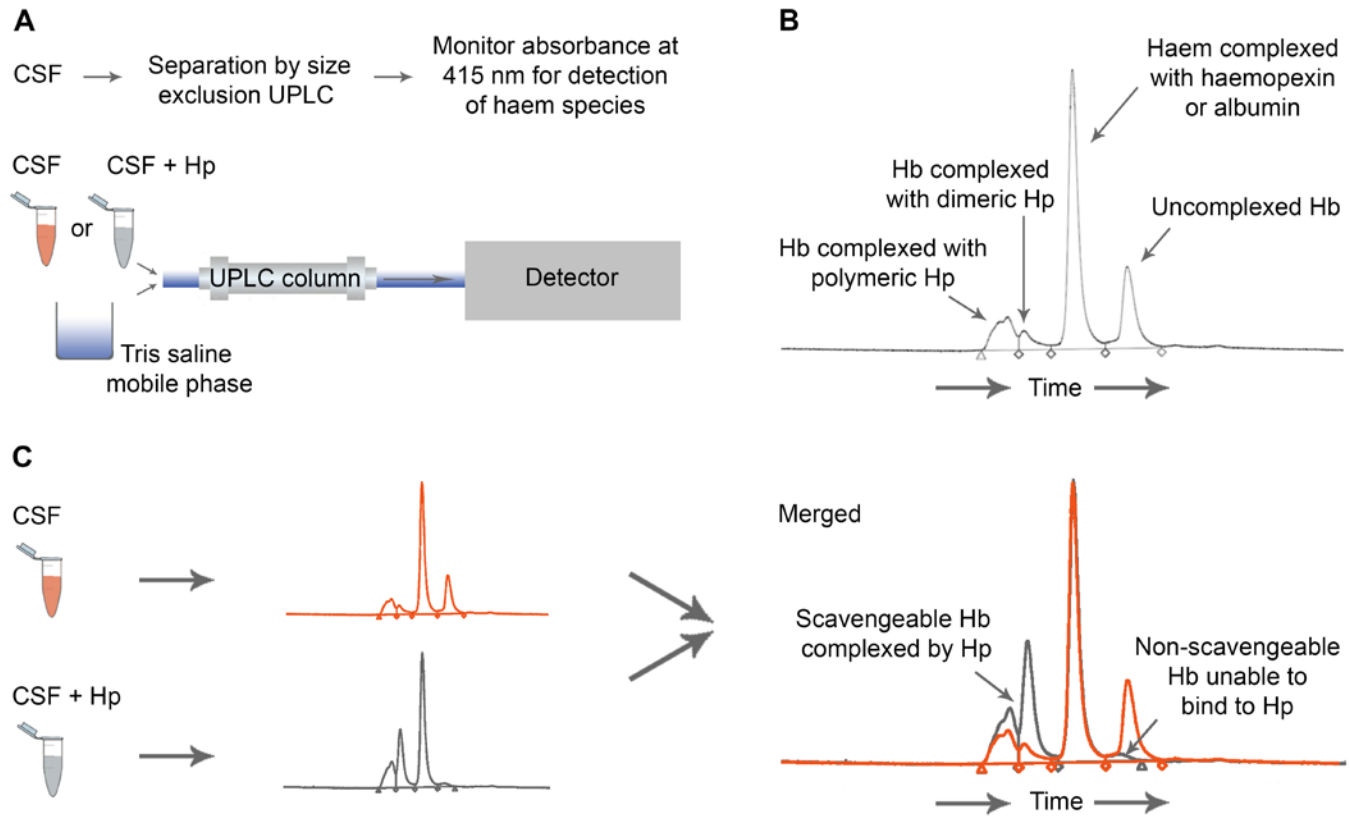

Figure 2. Human study

Hb predicts NFL concentration in the CSF of SAH patients. **a**, Peak NFL concentration is significantly higher in the CSF of SAH patients (n=42) *versus* a non-inflammatory and non-haemorrhagic control population (n=19). Upper and lower limits were derived from the Ln normal distribution of the control population (mean ±95% CI, unpaired t test). **b**, The CSF concentration of total Hb and NFL increase over a two week period post-ictus (n=42; median ±interquartile range (IQR, shaded zone)). **c**, Peak Hb concentration preceding peak NFL concentration is significantly higher in SAH patients with high NFL (n=30) *versus* SAH patients with normal NFL (n=12) (mean ±95% CI, unpaired t test). **d**, Multivariable linear regression of peak NFL on preceding peak total Hb, controlling for WFNS, age, and sex (n=42, B=0.364 (95% CI:0.156-0.573), p=0.001). **e**, Uncomplexed Hb (Hb not bound to Hp). **f**, Uncomplexed Hb that can bind Hp (**e**,**f**, n=42, median with IQR). **a**,**c**, p values $^{**}p < 0.01$, $^{****}p < 0.0001$.

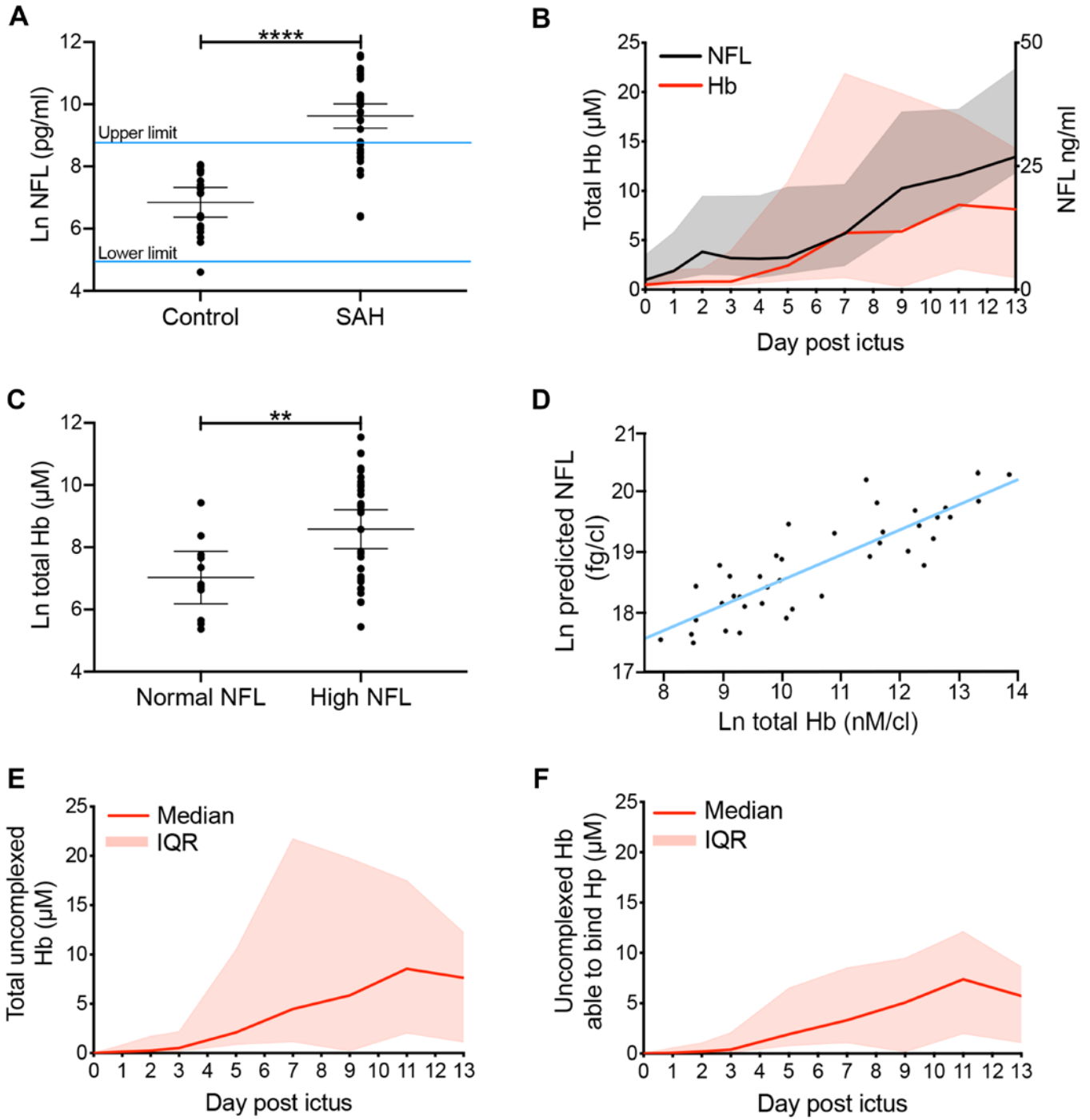

Figure 3. *In vitro* study

Hp reverses Hb toxicity towards mouse hippocampal neurones. **a**,**b**, Representative images of MAP2-positive neurones challenged for one week with vehicle or 10µM mouse Hb. **c**, Increasing concentration of Hb reduces the number of MAP2-positive neurones (n=5 experiments each with duplicate wells per condition, mean ±SEM, one-way ANOVA $p<0.0001$, p values for multiple comparisons are from Dunnett's test). **d**, An equimolar-binding ratio of Hp fully reverses a one-week 15µM Hb challenge (n=5 experiments each with duplicate wells per condition, mean ±SEM). Two way ANOVA: Hb x Hp interaction $p=0.0032$. **a**, Scale bar = 100µm. **c**,**d**, p values $^{**}p < 0.01$, $^{***}p < 0.001$

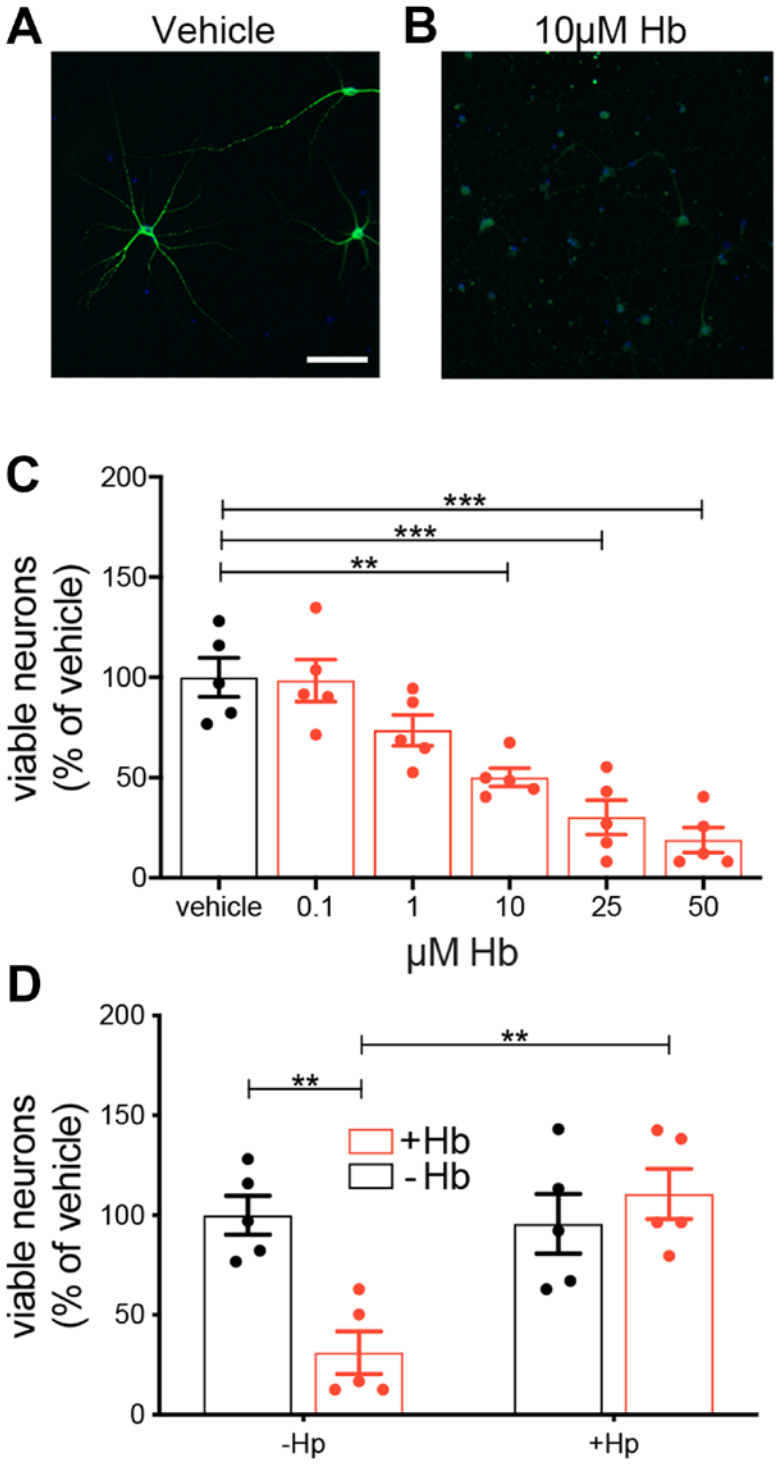

Figure 4. *In vivo* animal model: behaviour

Hp reverses behavioural deficits resulting from intracerebroventricular infusion of Hb. **a**, Experimental timeline. Mice were habituated to the open field and weighing apparatus for three days prior to surgery. Data from the day before surgery was taken as baseline. Post-surgery weight and open-field behaviour were assessed from day 2 until day 13. **b**, Ventricular cannula and osmotic minipump placement. **c**, Daily assessment of animal weights following surgery over the two-week experiment (saline: n=10, Hb: n=13, Hb+Hp: n=13, Hp: n=9). **d**, Representative images of Perls' staining, showing iron deposition. **e**, Representative traces following a five-minute open-field assessment. **f,** Linear-mixed modelling analysis of time-series data for ambulation performance in the open-field (saline: n=11, Hb: n=16, Hb+Hp: n=15, Hp: n=9). Hb x Hp interaction p=0.049. **g**, Linear-mixed modelling analysis of time-series data for freezing i.e. period spent immobile in the periphery of the open-field arena in the first minute (saline: n=11, Hb: n=16, Hb+Hp: n=15, Hp: n=9). Hb x Hp interaction p=0.065. **c**,**f**,**g**, mean ±SEM. **f**,**g**, p values *$p < 0.05$, ***$p < 0.001$. Scale bar = 500μm.

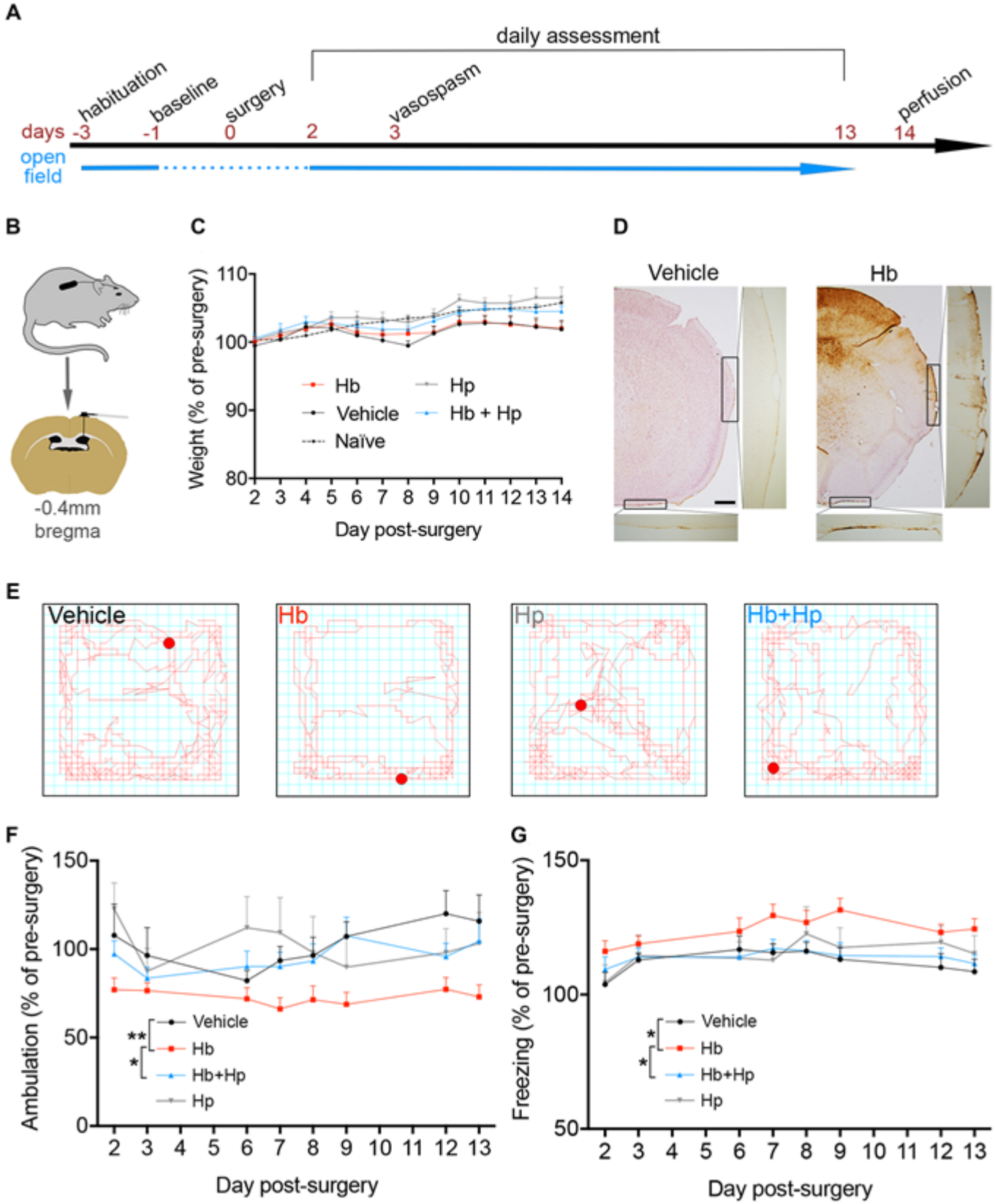

Figure 5. *In vivo* animal model: histology

Hp reverses changes in immunohistochemical markers of inflammation, injury, and synapse loss following prolonged intrathecal Hb exposure. **a**, Sampling sites (blue squares). **b**,**c**,**d**,**e**, Log(10) transformed counts of Iba1-positive cells in the cortex show an increase following Hb infusion, which was reduced to control levels with Hp treatment (n=7-13 per condition). Two-way ANOVA: Hb x Hp interaction p=0.003. **f**,**g**,**h**,**i**, Iba1-positive cells in the hippocampal molecular region (n=7-11 per condition). Two-way ANOVA: main effect for Hb p=0.04. **j**,**k**,**l**,**m**, GFAP-positive cells in the hippocampal molecular region show an increase following Hb infusion, which is reduced to control levels by Hp treatment (n=8-13 per condition). Two-way ANOVA: Hb x Hp interaction p=0.026. **n**,**o**,**p**,**q**, Sy38 (synaptophysin) staining across the hippocampal layers shows a reduction after Hb, which is reversed by Hp treatment (n=8-11 per condition). Two-way ANOVA: Hb x Hp interaction p=0.07. **b**,**f**,**j**, scale bar = 50µm. **n**, scale bar = 100µm. **e**,**i**,**m**,**q**, mean ±SEM, p values *$p < 0.05$, **$p < 0.01$, ***$p < 0.001$.

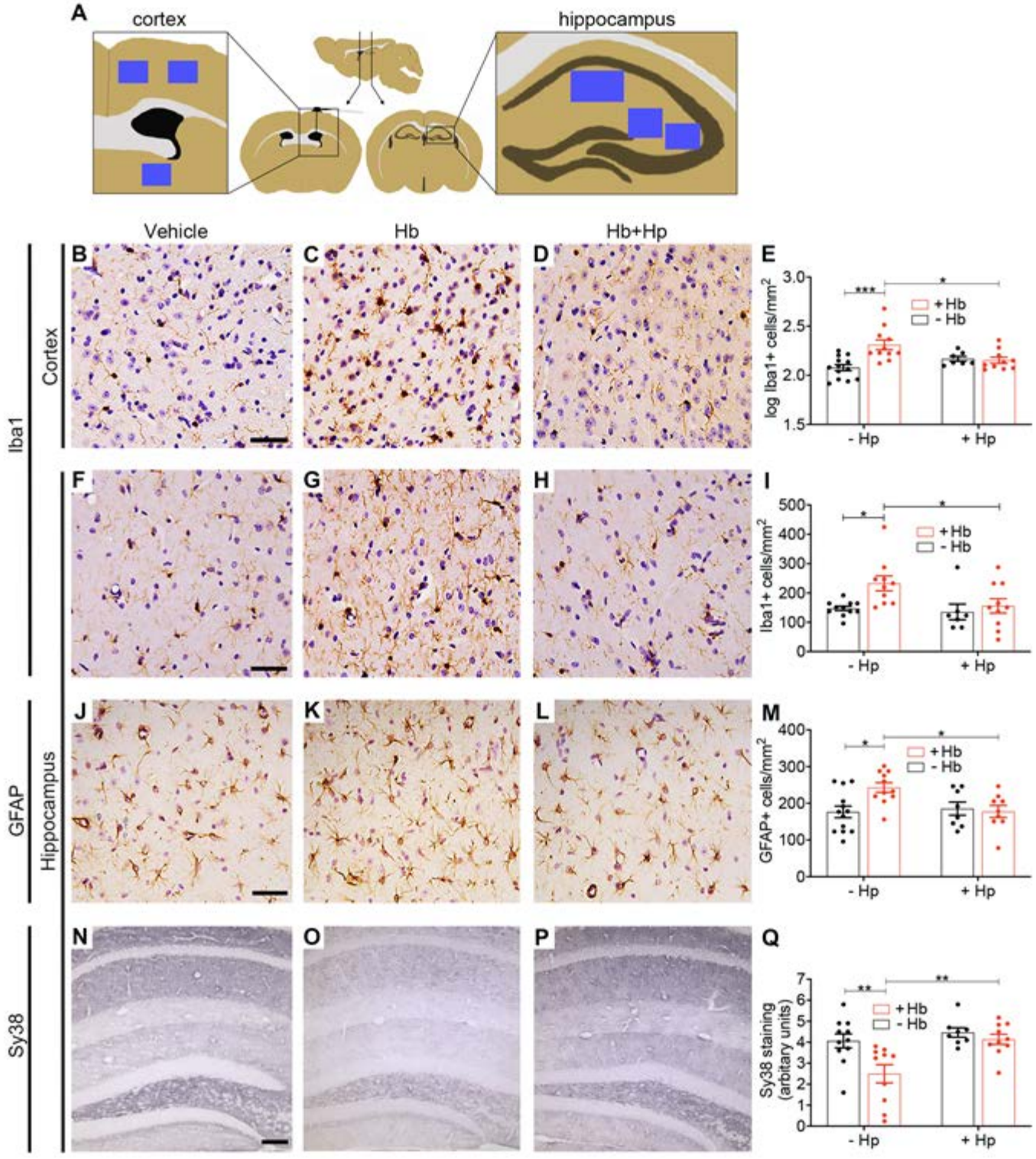

Figure 6. *In vivo* animal model: CD163 & iron

Top panel – Immunohistochemical analysis of CD163 expression. **a**, At three & 14 days post-surgery, both parenchymal and convexity staining for CD163 was unchanged between experimental groups (n=8-13, median ±interquartile range (IQR)).

Middle panel – Assessment of mixed-species Hp to Hb binding. **b**,**c**, Surface plasmon resonance analysis shows human Hp (hHp) does not augment binding of mouse Hb (mHb) to mouse CD163 (**b**), but hHp does increase binding of human Hb (hHb) to human CD163 (**c**).

Bottom panel – Hp reverses Perls' staining following intrathecal infusion of Hb. **d**, Perls' staining in the ipsilateral parenchyma at 14 days is significantly increased following Hb infusion, which is fully reversed by Hp (n=8-12, Kruskal-Wallis p=0.0002, median ±interquartile range (IQR)). **e**, Perls' staining on the brain surface and outer layers of the cortex on the ipsilateral side is significantly increased following Hb infusion (n=8-13, Kruskal-Wallis p=0.0003, median ±interquartile range (IQR)), which is decreased by Hp. **d**,**e**, *p* values **p* < 0.05, ****p* < 0.001.

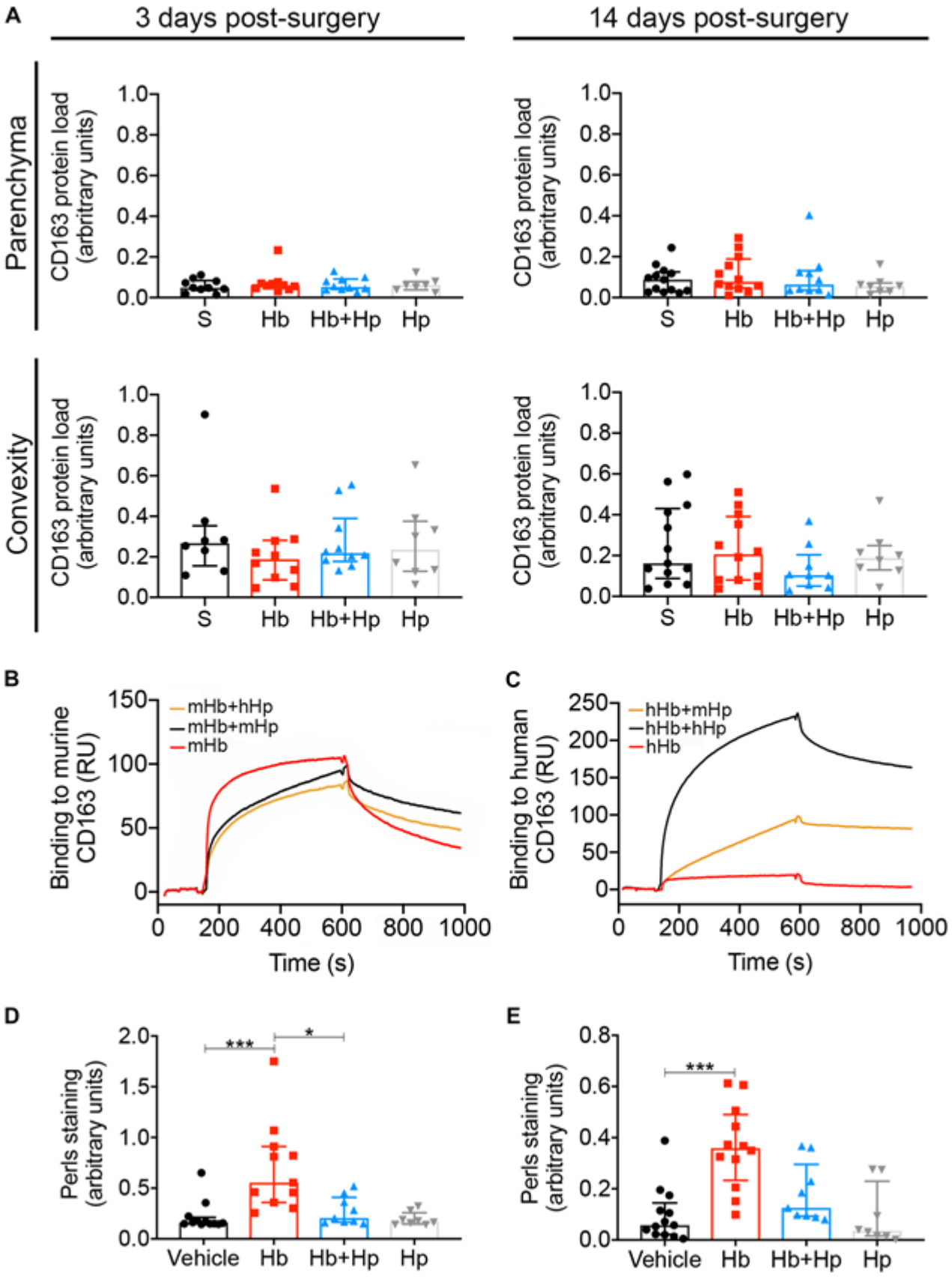

Figure 7. *In vivo* animal model: vasospasm

Large vessel – Intrathecal infusion of Hb for three days results in vasospasm of the middle-cerebral artery (MCA). **a**, Illustration of Circle-of-Willis and sampling area. **c**, Hb decreases ipsilateral MCA diameter, and this is unaffected by Hp. Two-way ANOVA: main effect Hb = 0.0058 (n=11, mean ±SEM). **f**,**g**,**h**, Representative images of MCA *in situ*. Scale bar = 100μm. **c**, *p* value $*p < 0.05$.

Small vessel – Hp reverses small-vessel vasospasm resulting from intrathecal infusion of Hb. **b**, Illustration of parenchymal sampling areas and method to determine vasoconstriction. **d**, Hp significantly reverses vasospasm in ipsilateral SMA+ vessels caused by a three day intrathecal Hb infusion. Two-way ANOVA: Hb x Hp interaction p=0.0182 (n=11, mean ±SEM). **e**, Immunohistochemical staining for Hb reveals a significant increase in the ipsilateral parenchyma after a three day Hb infusion, which is fully reversed by Hp (n=10-11, Kruskal-Wallis p=0.0001, median ±interquartile range (IQR)). **i**,**j**,**k**, Representative confocal images of SMA+ vessels in the ipsilateral parenchyma. Inset images are confocal slices at higher magnification (x20). Scale bar = 50μm. **d**,**e**, *p* values $*p < 0.05$, $**p < 0.01$.

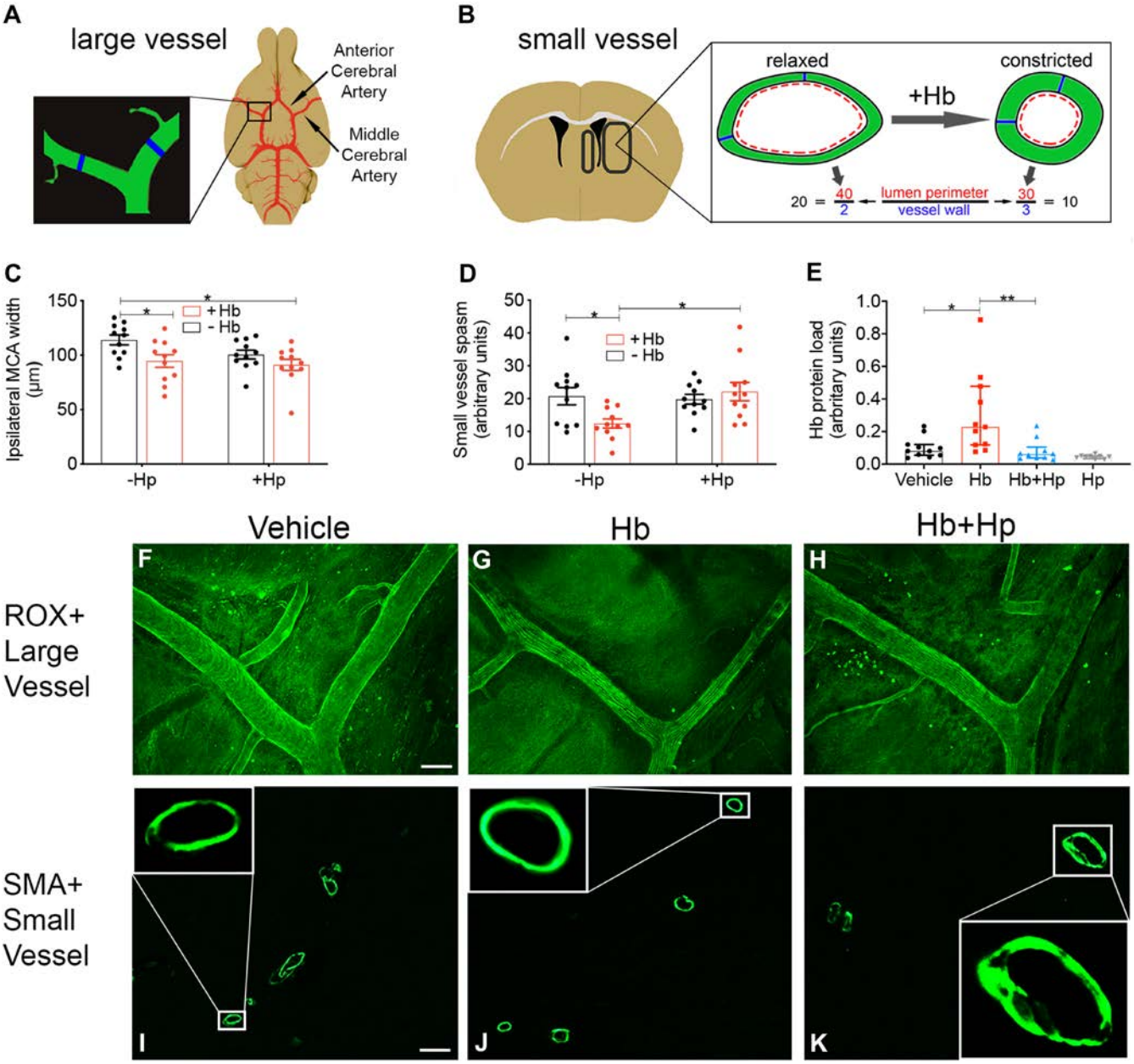

Table 1. Demographic and clinical characteristics of the clinical cohort. Mean & standard deviation[a], number and %[b]. The WFNS (World Federation of Neurological Surgeons) score describes the initial neurological condition.

	Non-traumatic SAH patients	**Control patients**
Number	44	19
Age (years)[a]	59.8 ± 12.3	55.2 ± 25.9
Gender[b] male female	 15 (34%) 29 (66%)	 5 (26%) 14 (79%)
Hypertension[b] Yes No	 23 (52.3%) 21 (47.7%)	
Initial WFNS (World Federation of Neurological Surgeons) score[b] 1 2 3 4 5	 5 (11.4%) 10 (18%) 6 (13.6%) 15 (29.5%) 8 (13.6%)	
Fisher grade[b] 3 4	 2 (4.5%) 42 (95.5%)	
Aneurysmal management[b] Coiled Clipped Supportive	 32 (72.7%) 5 (11.4%) 6 (13.6%)	
Aneurysm location[b] Anterior circulation Posterior circulation Perimesencephalic Unknown	 32 (72.7%) 7 (15.9%) 4 (9.1%) 1 (2.3%)	

Supplementary Material for

Haemoglobin causes neuronal damage *in vivo* which is preventable by haptoglobin

Patrick Garland[1], Matthew J Morton[1,*], William Haskins[1,*], Ardalan Zolnourian[2], Andrew Durnford[2], Ben Gaastra[2], Jamie Toombs[3,4], Amanda J Heslegrave[3,4], John More[5], Azubuike I Okemefuna[5], Jessica L Teeling[6], Jonas H Graversen[7], Henrik Zetterberg[3,4,8,9], Soren K Moestrup[7,10,11,#], Diederik O Bulters[2,#], Ian Galea[1,2,#,ψ]

* these authors contributed equally
# joint senior authors
ψ corresponding author: I.Galea@soton.ac.uk

[1] Clinical Neurosciences, Clinical & Experimental Sciences, Faculty of Medicine, University of Southampton, Southampton, United Kingdom
[2] Wessex Neurological Centre, University Hospital Southampton NHS Foundation Trust, Southampton, United Kingdom
[3] UK Dementia Research Institute, University College London, UK
[4] Department of Neurodegenerative disease, Institute of Neurology, London, UK
[5] R&D, Bio Products Laboratory Limited, Elstree, Hertfordshire, United Kingdom
[6] Biological Sciences, Faculty of Environmental and Life Sciences, University of Southampton, Southampton, United Kingdom
[7] Department of Molecular Medicine, University of Southern Denmark, 5000 Odense, Denmark
[8] Department of Psychiatry and Neurochemistry, Institute of Neuroscience and Physiology, The Sahlgrenska Academy at the University of Gothenburg, Mölndal, Sweden
[9] Clinical Neurochemistry Laboratory, Sahlgrenska University Hospital, Mölndal, Sweden
[10] Department of Clinical Biochemistry and Pharmacology, Odense University Hospital, 5000 Odense, Denmark
[11] Department of Biomedicine, Aarhus University, Aarhus, Denmark

This PDF file includes, in this order:

Supplementary Materials and Methods

Analysis of Hb in CSF from SAH patients

Human studies have been performed in accordance with the ethical standards as laid down in the 1964 Declaration of Helsinki. 44 Fisher grade III-IV SAH patients, requiring an external ventricular drain (EVD) as part of their clinical management, were recruited (National Research Ethics Committee approval number 12/SC/0666). CSF was obtained from the EVD on alternate days until removal of the EVD on day 13 (or earlier if clinically indicated). CSF was sampled on alternate days. Four patients died during the study and one of these patients had one CSF sample taken only, so this patient was not included in the analysis. Another patient had the EVD removed very early such that only one CSF sample was taken, and therefore this patient was not included either. Hence only 42 patients contributed to the study. CSF was drawn from a three way tap connecting the ventricular catheter (approximately 30cm long) to the tubing leading to an external CSF drainage and monitoring system (Becker®, Medtronic). For sampling, the tap was opened to the ventricular catheter, and closed to the drainage system. The first 3ml of CSF (representing dead space) was discarded to ensure fresh CSF was obtained. CSF was centrifuged at 1500 rcf for 10 minutes at 21°C and frozen within one hour of sampling. UPLC was used to separate CSF components in a tris-saline mobile phase. Eluate absorbance was measured at 415 nm to identify haem-containing species. CSF from individuals undergoing lumbar puncture for non-haemorrhagic neurological indications (National Research Ethics Committee reference no: 11/SC/0204) and a standard Hb solution (Sigma-Aldrich, Gillingham, Dorset, UK) confirmed the specificity of absorbance at 415nm to haem-containing species. The identity of the peaks on the UPLC chromatogram was confirmed by running the following reagents in combination with Hb/hemin: haemopexin (Sigma-Aldrich, Gillingham, Dorset, UK), Hp (Bio Products Laboratory Ltd. (BPL), Elstree, UK) and sera from Hp1-1, 2-1 and 2-2 individuals whose Hp phenotype was determined by western blotting (Galea *et al.*, 2012). To quantify Hb, a standard curve (nine data points from 0 to 1 g/l) was prepared from lyophilized human Hb (Sigma-Aldrich, Gillingham, Dorset, UK) reconstituted to 1g/L in diluent (9 g/L NaCl, 10 mM EDTA), and absorbance measured at 415 nm after UPLC. The concentration of the standard Hb solution was verified independently by spectrophotometric quantification at 570 nm using Hemocue™ (Hemocue, Sweden). Hb was measured in CSF before and after saturating with Hp (BPL, Elstree, UK) to measure Hp-bindable and Hp-unbindable uncomplexed Hb (Fig. 1). 50µl of each sample was loaded onto

the UPLC column (Acquity BEH C18, #186005225, Waters, Waters, Elstree, Herts, UK) using a running buffer consisting of 50 mM Tris and 150 mM NaCl, at pH 7.5. Absorbance was measured at 415 nm, the area under the curve was quantified and Hb concentration was calculated using the standard curve. Each assay run was quality controlled using three in-house Hp standards (200 μg/ml, 10 μg/ml and 1 μg/ml) covering the assay range.

Control individuals

Control participants were patients who underwent lumbar puncture for neurological symptoms or conditions which were non-inflammatory and non-haemorrhagic (e.g. headache, normal pressure hydrocephalus and idiopathic intracranial hypertension) and were confirmed to have normal CSF. The National Research Ethics Committee approval number was 11/SC/0204.

Measurement of CSF neurofilament light chain

NFL was measured by enzyme-linked immunosorbent assay (UmanDiagnostics, Umea, Sweden), according to the manufacturer's instructions. Briefly, samples were thawed at 21°C, and centrifuged at 1750 rcf for 5 minutes at 21°C. Samples were then diluted 1:2 with sample diluent and added in duplicate to microplate wells coated with a monoclonal capture antibody specific for NFL. Next, samples were incubated with a biotinylated NFL-specific monoclonal detection antibody. The detection complex was completed with the addition of horseradish peroxidase-labelled streptavidin and tetramethylbenzidine (TMB) substrate. Samples were read at 450nm. Sample concentrations were extrapolated from a standard curve, fitted using a 4-parameter logistic algorithm. Intra-assay CVs were less than 10%.

Preparation of Hb from mouse RBCs

Blood was collected from C57BL/6 mice following administration of a terminal dose of pentobarbital. In a laminar flow hood, 5ml of blood was brought to 15ml using phosphate-buffered saline (PBS) (#20012-019, Thermo Fisher, Loughborough, UK) and centrifuged at 480g for 15 minutes. The supernatant was removed using aspiration, which included carefully removing the buffy coat. This centrifugation/resuspension/aspiration procedure was repeated three times until the supernatant was clear and the leukocyte layer fully depleted, leaving 2ml of RBC containing solution. 1.5ml of this solution was removed by pipetting from the bottom of the tube and brought to 6ml using sterile, distilled water (#UKF7114, Baxter, Newbury, Berkshire). Following gentle and brief mixing, RBC ghost membranes were pelleted via a

13,000g centrifugation for 30 minutes. The Hb containing supernatant was collected and brought to 0.9% NaCl using a 10X stock solution (made using sterile water and filtered through a 0.45µm filter). This final solution was then passed through a 0.45µm filter. Protein content was determined using the bicinchoninic acid assay (#23227, Thermo Fisher, Loughborough, UK). Hb constitutes 98% of total RBC cytosolic protein (Liumbruno *et al.*, 2010; Lutz and Bogdanova, 2013), and the purity of each preparation was assessed by sodium dodecyl sulphate polyacrylamide gel electrophoresis and Coomassie staining (Supplementary Figure 7).

Primary neuronal cultures

Primary hippocampal neurones were cultured according to a modified method from the Ittner lab (Fath *et al.*, 2009; Garland *et al.*, 2012). This method utilizes a support ring of cortical cells in the periphery of a culture dish to provide trophic support to a low-density culture of hippocampal neurones on a central coverslip. Briefly, postnatal day 0 C57BL/6 mice were sacrificed and their hippocampal and cortical neurones dissociated using a kit designed for postnatal neurones (#130-094-802, Miltenyi, Bisley, Surrey, UK). Cortical and hippocampal cells were suspended in growth media (Neurobasal & 1X GlutaMAX, Thermo Fisher, Loughborough, UK; 1X Neurobrew, Miltenyi, Bisley, Surrey, UK) and plated at the following densities: 250,000/75µl cortical cells for the support ring, and 5000/50µl hippocampal cells per coverslip in 12 well plates. After four hours, suspension media was removed and replaced with 1 ml of pre-equilibrated growth media. Every 3–4 days 50% of culture media was replaced with fresh and pre-equilibrated growth media. Cultures were maintained at 5% CO_2 and 37^{o}C, and used after seven days.

Immunocytochemistry

Cultured neurones were washed in PBS and fixed for 30 minutes with 4% paraformaldehyde (PFA). Following two five-minute washes with PBS, neurones were incubated at 21°C with blocking buffer (BB) (made of 5% normal goat serum, 1% BSA and 0.2% Triton X-100 in PBS), and then incubated with anti-MAP2 (1:500; #AB5622, Millipore, Merck, Watford, Hertfordshire, UK) overnight at 4^{o}C in BB. Wells were washed with PBS three times, for five minutes each wash, and incubated with anti-rabbit Alexa488 (Thermo Fisher, Loughborough, UK) in PBS for one hour. Wells were then washed with PBS three times, for five minutes each wash. Coverslips were mounted onto glass slides using Prolong Gold with DAPI (#P36941, Thermo Fisher, Loughborough, UK).

Hb challenge and Hp treatment

Cultured neurones were challenged with Hb at day 7 until day 14. Over the 7 days, Hb concentration was maintained during media changes. An equimolar-binding ratio of Hp was added concomitantly for Hp treatment experiments.

Counting viable neurons

Following blinding, coverslips were imaged using a Leica DM5000 microscope under x40 magnification. The objective was passed over the full length of each coverslip and viable neurones identified as MAP2-positive with non-apoptotic nuclei. The mean from 2 coverslips for each repeat was taken.

Source of haptoglobin

Hp was purified from pooled human plasma at Bio Products Laboratory Limited (http://www.bplgroup.com), with a methodology (Dalton, 2012) that enriches for Hp dimer (Lipiski *et al.*, 2013) (dimer, 68%; trimer, 16%, higher polymeric forms, 16%); it was 98% pure as determined by UPLC. The preparation used in this study was a clinical grade formulation with <0.02 endotoxin units/ml. The Hb-binding capacity of this Hp preparation was determined empirically by incubating increasing concentrations of mouse Hb with a fixed concentration of Hp (1mg/ml), followed by UPLC quantification (Supplementary Figure 8). Binding was observed to saturate at a Hb to Hp mass ratio of 1:1.4.

Mouse model of prolonged intrathecal Hb exposure

To model prolonged intrathecal Hb exposure, a two-week intracerebroventricular infusion of Hb was used. Locally bred male C57BL/6 mice were housed at 21ºC under a 12-hour light/12-hour dark cycle in a conventional animal research facility, and allowed access to food and water *ad libitum*; surgery was performed at 10-12 weeks of age. All procedures were performed under U.K. Home Office licence 30-3057 and all applicable international, national, and/or institutional guidelines for the care and use of animals were followed. Alzet osmotic minipumps (Model 2002, #296, two-week infusion, 0.5µl/hr, Charles River, Harlow, Essex) were loaded with vehicle (0.9% saline), Hb, Hb + Hp, or Hp. Treatment allocation was random. The infusate Hb concentration was 20mg/ml. To achieve a clinically relevant CSF Hb concentration of 10µM, the following parameters were used to guide optimization of the infusate Hb concentration: CSF volume in mice = 40µL (Rudick *et al.*, 1982); CSF formation rate = 0.33µL/min (Rudick *et al.*, 1982); C57BL/6J mouse brain weight = 0.45g (Rosen and Williams, 2001); interstitial fluid (ISF) is 20% of brain weight (Davson and Segal, 1996); rate

of ISF formation 0.17µL/g/min in rodents (Cserr *et al.*, 1981; Abbott and Bradbury, 1992). The Hp concentration was 14mg/ml to achieve 1:1 Hb to Hp binding stoichiometry, guided by data from empirical determination of Hb to BPL Hp binding ratio (Supplementary Figure 8). The minipump was attached to a 30-gauge ventricular cannula using vinyl tubing (Brain Infusion Kit 3, #8851, Charles River, Harlow, Essex), and primed with test solution according to the manufacturer's instructions. Mice were anaesthetised using a ketamine (Bayer, Reading, UK) and xylazine (Pfizer, Tadworth, Surrey, UK) mixture (100 and 10 mg/kg, respectively). The head was immobilized in a stereotactic frame. Mice body temperature was thermostatically controlled with a rectal probe and a heated pad. An aseptic technique was used. Blunt dissection was used to create a subcutaneous pocket in the interscapular region for insertion of the minipump. A burr hole was drilled and the ventricular cannula inserted at the following coordinates from bregma: anteroposterior, -0.4mm; lateral, 1mm; depth, 2.5mm. Cyanoacrylate was used to secure the cannula holder to the skull surface. Buprenorphine (Centaur, Castle Cary, Somerset, UK) was administered immediately following surgery (0.5mg/kg subcutaneously) and the next morning in 5ml fruit jelly (300µg/45ml). Mice were housed individually following surgery for 14 days so the experimental unit was a single animal. Mice were checked twice in the first 24 hours and daily thereafter. Residual volume in the minipumps was systematically examined after explantation, at the end of the two weeks, to ensure the appropriate volume of 200µL was delivered while *in situ*. Correct placement of the ventricular cannula was confirmed during tissue sectioning by observing the cannula track.

Open-field behavioural analysis

Open-field behavioural analysis was performed in a laser-monitored behaviour arena (Med Associates, Fairfax, VA, US) over a five-minute period, twice a day at the same time in the morning and afternoon. An ambulation score was calculated by combining the percentage change from baseline for three ambulatory readouts: distance travelled, ambulatory counts, and time spent ambulating. A freezing score was calculated by deriving the percentage change from baseline for the time spent in the outer 25% of the open field over the first minute (Supplementary Figure 9).

Immunohistochemistry

At 14 days post-surgery, mice were transcardially perfused with heparinised saline (1unit/ml, LEO Pharma, Hurley, Berkshire, UK), followed by 4% PFA in 0.1M phosphate buffer. Brains

were removed and post-fixed in 4% PFA overnight at 4°C and then embedded in paraffin wax. Coronal sections were cut at 10µm, dewaxed in xylene, and rehydrated through graded ethanol/water solutions. Protocols for each marker were as follows:

GFAP/Iba1

For antigen retrieval, sections were immersed in 10mM citrate buffer (pH6) and boiled in a microwave for 6 minutes. Endogenous peroxide was quenched using 0.3% v/v hydrogen peroxide in 1% v/v methanol for 30 minutes. Sections were blocked in 5% v/v normal goat serum + 0.1% w/v BSA for one hour at RT. In the same blocking solution, sections were incubated at 4°C overnight with primary antibody (1:500 anti-Iba1, Wako, Osaka, Japan; 1:2000 anti-GFAP, Dako, Agilent, Santa Clara, CA, US). Following three five-minute washes in PBS with 0.1% Tween-20 (PBS-T), sections were incubated with biotinylated anti-rabbit antibody (1:100, #BA-1000, Vector labs, Burlingame, CA, US) for one hour at RT in PBS. Sections were washed in PBS-T three times, for five minutes each wash, and then incubated in ABC solution (#PK-6100, Vector Labs, Burlingame, CA, US) for 45 minutes at RT. Sections were washed in PBS three times, for five minutes each wash, followed by development in 0.1M phosphate buffer containing 0.05% w/v 3,3'-Diaminobenzidine and 0.015% v/v hydrogen peroxide. Sections were counterstained in haematoxylin, dehydrated through graded ethanol/water solutions, cleared in xylene, and mounted using DPX.

Synaptophysin

For antigen retrieval, sections were incubated at 65°C in 0.2M boric acid (pH9) for 30 minutes. Endogenous peroxide was quenched using 0.3% hydrogen peroxide in PBS. Sections were blocked in 10% normal goat serum for one hour at RT in PBS and then incubated with anti-synaptophysin (1:2000, UK #5258-I, Millipore, Merck, Watford, Hertfordshire) in the same blocking solution overnight at 4°C. Sections were washed in PBS with PBS three times, for five minutes each wash, and then incubated with biotinylated anti-mouse antibody (#9200, Vector Labs, Burlingame, CA, US) in PBS for one hour at RT. Sections were washed in PBS three times, for five minutes each wash, and incubated with ABC solution for 45 minutes. Finally, sections were washed in PBS three times, for five minutes each wash, followed by development in 0.1M phosphate buffer containing 0.05% w/v 3,3'-Diaminobenzidine, 0.015% v/v hydrogen peroxide, and 0.06% w/v ammonium nickel sulphate. Sections were dehydrated through graded ethanol solutions, cleared in xylene, and mounted using DPX without counterstaining.

Haemoglobin/CD163

Sections were boiled in a citrate buffer (10mM, pH6) for two five-minute heat/cool cycles, washed twice for five minutes in PBS, and quenched in 3% hydrogen peroxide for 10 minutes in PBS. After two five-minute washes in PBS, sections were blocked with 10% goat serum + 1% BSA in PBS for one hour at RT. Blocking buffer was tapped off, and sections incubated in 1/500 anti-Hb (ab102758, Abcam, Cambridge, UK) or 1/500 anti-CD163 (ab182422, Abcam, Cambridge, UK) overnight at 4^{o}C. Sections were washed in PBS three times, for five minutes each wash, and subjected to the DAB method as per section for 'GFAP/Iba1'. Both unstained and counterstained sections were prepared prior to mounting in DPX.

Smooth muscle actin

Fixed-frozen sections were warmed for 15min at 37^{o}C and then blocked in 10% normal goat serum for 30min in PBS. Blocking buffer was tapped off and sections incubated with 1/100 anti-SMA-FITC (F377, Sigma-Aldrich, Gillingham, Dorset, UK) overnight in PBS+0.1% triton X-100 at 4^{o}C. Sections were washed in PBS three times, for five minutes each wash, and mounted using Prolong Gold antifade reagent with DAPI (P36941, Thermo Fisher, Loughborough, UK).

Fluorescent imaging of Circle of Willis in situ

The method for *in situ* imaging was established in the Zipfel group (Aum *et al.,* 2017). Mice were anaesthetised using a ketamine (Bayer, Reading, UK) and xylazine (Pfizer, Tadworth, Surrey, UK) mixture (100 and 10mg/kg, respectively) and transcardially perfused through the left ventricle with 10mM glucose-PBS followed by 20 mL 20μM 5-(6)-carboxy-X-rhodamine, succinimidyl ester (ROX SE, Sigma-Aldrich, Gillingham, Dorset, UK) dye in 10mM glucose-PBS prior to perfusions with 4% PFA (in PBS). All perfusions were performed with solutions at 21°C, at a constant pressure of 80mmHg ±2mmHg using a GE Druck DP1705. Animals were decapitated, the calvaria removed, and post-fixed in 4% PFA in the dark at 4°C for 24 hours. Brains were removed under a dissection microscope to preserve the basal arteries. Then, brains were placed *en bloc* on a glass coverslip and gently covered in PBS before placing on the stage of a confocal laser scanning microscope (SP8, Leica, Wetzlar, Germany). Vessels were imaged at 1024 x 1024 pixel resolution with four line averaging, 10x magnification and 0.75 zoom using an excitation laser wavelength of 561 nm and monitoring emittance between wavelengths of 572 –699 nm. Z stacks were generated through the entire vessel with spacing of 10μm. The z stack data were visualized in two dimensions using the maximum projection function. Photomicrographs were acquired of the Anterior Cerebral Artery (ACA) and Middle Cerebral

Artery (MCA). Measurements of vessel diameter were made in ImageJ (National Institute of Health, USA) using the line tool and measure function by drawing from one wall of the vessel to the other in a perpendicular direction. Measurements were made at the narrowest point across the first 1 mm of the vessel.

Perls' staining

Following de-waxing, slides were rehydrated through graded ethanol/water solutions and then incubated at 40ºC in 7% w/v potassium ferrocyanide and 2% v/v hydrochloric acid mixed in a 1:1 ratio for 1hr. After a brief wash in distilled water, endogenous peroxidase activity was quenched in 0.3% v/v hydrogen peroxide in Tris-buffered saline for 30 minutes at RT. Sections were developed in 0.1M phosphate buffer containing 0.05% w/v 3,3'-Diaminobenzidine and 0.015% v/v hydrogen peroxide for seven minutes. Of the three sections per slide, only two were counterstained with haematoxylin; the unstained section was used for quantification of Perls' staining. Sections were dehydrated through graded ethanol/water solutions and cleared in xylene prior to mounting with DPX.

Imaging

To ensure blinding, all samples were coded prior to image capture and analysis. Images were captured using a Leica DM5000 microscope. Images were captured from the hemisphere ipsilateral to the cannula. All analyses were performed by two-dimensional quantification, averaged over two sections per animal within each area studied, and data is presented per mm^2, unless otherwise indicated.

GFAP/Iba1

Images were captured under x40 magnification. Two main sampling regions were selected to represent the cortex/thalamus and the hippocampus caudal to the Hb infusion site. Each region was sub-sampled in three areas in a standardized way (Supplementary Figure 10A). For the first region, two sample sites were in the cortex and one in the thalamus. For the hippocampal region, one central sample site was within the hippocampal molecular layer, in between CA1 and CA3 sample sites within the stratum radiatum adjacent to the pyramidal cell layer. Cells positive for each marker were counted from two sections from each location.

Synaptophysin

Brightfield images were taken at x10 magnification in order to image multiple strata of the ipsilateral hippocampus. Synaptophysin staining was quantified using the method established

by Cunningham *et al* (Cunningham *et al.*, 2003), to quantify staining as a ratio between regions normalised to the background staining intensity. Briefly, hippocampal strata pixel densities were measured using ImageJ software (National Institute of Health, USA) with measurements made at a light intensity within the linear transmittance (T) range. The dentate gyrus (DG) granular cell layer (the area of highest transmittance) was used as an internal control for each section and other strata transmittances were adjusted by subtraction of the DG transmittance from this layer's transmittance. A ratio was then calculated using the adjusted transmittances for the SR (the most variably stained regions) and the SLM (a consistently low stained region): Ratio = $(T_{DG} - T_{SR})/(T_{DG} - T_{SLM})$. Two sections per animal were analysed and a mean ratio calculated.

Smooth-muscle actin

Fluorescent images were captured under x10 magnification. Two sites either side of the ipsilateral lateral ventricle were used. Between 4-6 SMA+ vessels in a transverse orientation were imaged per animal resulting in ≈200 vessels being analysed across all groups. In ImageJ, each vessel was magnified and its lumen diameter and wall thickness measured. A ratio of lumen perimeter to wall thickness was calculated (Sabri and Macdonald, 2012). There was not a specific vessel size range; only vessels strictly within the brain tissue (i.e. not in the leptomeninges) were analysed.

Haemoglobin

Images of non-counterstained sections were collected under brightfield microscopy at x10 magnification. Three images were taken for each animal in the ipsilateral hemisphere. Image analysis in ImageJ used the same macro as per 'Perls' staining' below.

Perls' staining

Brightfield images of non-counterstained sections were obtained at x20 magnification; the convexity was sampled at the base of the brain and lateral aspect (Supplementary Figure 10B); the parenchyma was sampled either side of the lateral ventricle (Supplementary Figure 10A). Analysis was carried out using ImageJ. Following conversion to 8 bit format, all images were subjected to the same thresholding. The area fraction of staining was then quantified to represent the degree of non-haem iron deposition.

Western blotting

The hemisphere ipsilateral to cannula insertion was homogenised in RIPA buffer. 20µg of protein was separated on TGX 4-15% gels (BioRad, Watford, Hertfordshire, UK) and

transferred onto PVDF using a Trans-Blot Turbo system (BioRad, Watford, Hertfordshire, UK). The membrane was blocked in 3% BSA in Tris-buffed saline (pH 7.4) containing 0.1% Tween-20 (TBS-T) for one hour at RT. Membranes were incubated at 4^{o}C overnight in the same blocking buffer containing 1:1000 mouse anti-postsynaptic density protein 95 (#ab13552, Abcam, Cambridge, UK), and 1:1000 mouse anti-tubulin β3 (#801201, Biolegend, San Diego, CA, US). Membrane was washed in TBS-T three times, for five minutes each wash, and incubated with and Alexa546-conjugated anti-mouse IgG (Invitrogen, Carlsbad, CA, US) for one hour at RT. Following three five-minute washes in TBS-T, the membrane was imaged using a ChemiDoc system (BioRad, Watford, Hertfordshire, UK) with exposure set to prevent saturated pixels.

Surface plasmon resonance

SPR analysis was carried out as described (Madsen *et al.*, 2004) using a Biacore 3000 instrument (Biacore, Uppsala, Sweden). Mouse or human CD163 (produced recombinantly in house (Kristiansen *et al.*, 2001; Etzerodt *et al.*, 2013)) were immobilized in 10mM sodium acetate (pH 4) and remaining binding sites were blocked with 1M ethanolamine (pH 8.5). The resulting densities were: human CD163 0.0468 pmol/mm^2, and murine CD163 0.0320 pmol/mm^2. Sensorgrams were generated using the running buffer CaHBS with 2mM free Ca_2Cl_2 (10mM Hepes, 150mM NaCl, 3.0mM $CaCl_2$, 1.0mM EGTA, + 0.005% P20, and pH 7.4) and the protein concentrations: 5µg/ml of mouse and human Hb (Sigma-Aldrich, Gillingham, Dorset, UK); 7.5 µg/ml of mouse Hp (MyBioSource, San Diego, Ca) and human Hp1-1 (Sigma-Aldrich, Gillingham, Dorset, UK). The flow cell was regenerated in 10mM glycine, 20mM EDTA, 500mM NaCl+0.005% P20, pH4.0 between the runs. All experiments were at least conducted in triplicate and data was evaluated using the BiaEvaluation ver. 4.1 software (Biacore, Uppsala, Sweden).

Statistics

The normal reference range for NFL was derived from control individuals by using the natural log normal distribution. Values were natural log transformed and the upper and lower limits were calculated as three standard deviations on either side of the mean. Where possible, experiments were conducted using a 2x2 factorial design to reduce the number of animals used (Festing *et al.*, 2016) in line with the principle of 3Rs (Festing *et al.*, 2016). These experiments were analysed with a two-way analysis of variance (ANOVA) considering Hp and Hb as

factors with two levels each. Kruskal-Wallis test was used for non-parametric factorial data. The three primary hypotheses were: (1) Hb is toxic (2) Hp is not toxic (2) Hp protects against Hb toxicity. Mice received four types of intrathecal infusions: Hb only (n=16), Hb with an equimolar-binding ratio of Hp (n=15), Hp alone (n=9) or vehicle (n=13). *p* values were corrected for multiple comparisons using the false discovery rate method (Benjamini and Hochberg, 1995) with Q=0.05; sensitivity analyses using the full pairwise Bonferroni correction showed results were robust (Supplemental Table 2). One-way ANOVA was used to study the toxicity of different Hb concentrations *versus* control, for which multiple comparisons were corrected using Dunnett's. Weighted Pearson's r was used to determine correlations. A linear-mixed modelling approach was used to analyse time-series behavioural data, with a first order ante dependence covariance structure used to model correlated terms under heteroscedasticity. Within-subject random effects were modelled using random intercepts. Model comparison was assessed using Akaike information criterion and the log-likelihood ratio. Normality and heteroscedasticity was routinely determined across all data sets. Where necessary, logarithmic transformation was used to normalise data. α, the probability of a Type I error, was 0.05. Two-tailed hypotheses were considered throughout. Statistical analysis and graph preparation were performed using SPSS (v24) and GraphPad Prism (v7.01), with data expressed as mean ± standard error of the mean (SEM), median ± interquartile range, or 95% confidence intervals. Supplemental Table 2 details all the analyses performed and the results. Animals were randomly selected and sequentially assigned to treatment groups. Animal *in vivo* experiments were reported according to ARRIVE guidelines, and the checklist is available as Supplemental data (Kilkenny *et al.*, 2010).

Supplementary References

Abbott NJ, Bradbury MWB. Physiology and pharmacology of the blood-brain barrier. Handbook of experimental pharmacology. Berlin; New York: Springer-Verlag; 1992. p. 549.

Aum DJ, Vellimana AK, Singh I, Milner E, Nelson JW, Han BH, *et al.* A novel fluorescent imaging technique for assessment of cerebral vasospasm after experimental subarachnoid hemorrhage. Sci Rep 2017; 7(1): 9126.

Benjamini Y, Hochberg Y. Controlling the False Discovery Rate: A Practical and Powerful Approach to Multiple Testing. Journal of the Royal Statistical Society Series B (Methodological) 1995; 57(1): 289-300.

Cserr HF, Cooper DN, Suri PK, Patlak CS. Efflux of radiolabeled polyethylene glycols and albumin from rat brain. Am J Physiol 1981; 240(4): F319-28.

Cunningham C, Deacon R, Wells H, Boche D, Waters S, Diniz CP, *et al.* Synaptic changes characterize early behavioural signs in the ME7 model of murine prion disease. Eur J Neurosci 2003; 17(10): 2147-55.

Dalton JO, Azubuike. Haptoglobin. In: Bertolini JG, Neil; Curling, John, editor. Production of Plasma Proteins for Therapeutic Use. Hoboken, New Jersey: John Wiley & Sons, Inc.; 2012.

Davson H, Segal MB. Physiology of the CSF and blood-brain barriers. Boca Raton: CRC Press; 1996.

Etzerodt A, Kjolby M, Nielsen MJ, Maniecki M, Svendsen P, Moestrup SK. Plasma clearance of hemoglobin and haptoglobin in mice and effect of CD163 gene targeting disruption. Antioxidants & redox signaling 2013; 18(17): 2254-63.

Fath T, Ke YD, Gunning P, Gotz J, Ittner LM. Primary support cultures of hippocampal and substantia nigra neurons. Nat Protoc 2009; 4(1): 78-85.

Festing MFW, Overend P, Borja MC, Berdoy M. The design of animal experiments: reducing the use of animals in research through better experimental design. 2nd edition / Revised and updated edition. ed. Los Angeles: SAGE; 2016.

Galea J, Cruickshank G, Teeling JL, Boche D, Garland P, Perry VH, *et al.* The intrathecal CD163-haptoglobin-hemoglobin scavenging system in subarachnoid hemorrhage. J Neurochem 2012; 121(5): 785-92.

Garland P, Broom LJ, Quraishe S, Dalton PD, Skipp P, Newman TA, *et al.* Soluble axoplasm enriched from injured CNS axons reveals the early modulation of the actin cytoskeleton. PLoS One 2012; 7(10): e47552.

Kilkenny C, Browne WJ, Cuthill IC, Emerson M, Altman DG. Improving bioscience research reporting: the ARRIVE guidelines for reporting animal research. PLoS Biol 2010; 8(6): e1000412.

Kristiansen M, Graversen JH, Jacobsen C, Sonne O, Hoffman HJ, Law SK, *et al*. Identification of the haemoglobin scavenger receptor. Nature 2001; 409(6817): 198-201.

Lipiski M, Deuel JW, Baek JH, Engelsberger WR, Buehler PW, Schaer DJ. Human Hp1-1 and Hp2-2 phenotype-specific haptoglobin therapeutics are both effective in vitro and in guinea pigs to attenuate hemoglobin toxicity. Antioxidants & redox signaling 2013; 19(14): 1619-33.

Liumbruno G, D'Alessandro A, Grazzini G, Zolla L. Blood-related proteomics. J Proteomics 2010; 73(3): 483-507.

Lutz HU, Bogdanova A. Mechanisms tagging senescent red blood cells for clearance in healthy humans. Front Physiol 2013; 4: 387.

Madsen M, Moller HJ, Nielsen MJ, Jacobsen C, Graversen JH, van den Berg T, *et al*. Molecular characterization of the haptoglobin.hemoglobin receptor CD163. Ligand binding properties of the scavenger receptor cysteine-rich domain region. The Journal of biological chemistry 2004; 279(49): 51561-7.

Rosen GD, Williams RW. Complex trait analysis of the mouse striatum: independent QTLs modulate volume and neuron number. BMC Neurosci 2001; 2: 5.

Rudick RA, Zirretta DK, Herndon RM. Clearance of albumin from mouse subarachnoid space: a measure of CSF bulk flow. J Neurosci Methods 1982; 6(3): 253-9.

Sabri M, Macdonald RL. Vasospasm: Measurement of Diameter, Perimeter, and Wall Thickness. In: Chen J, Xu X-M, Xu ZC, Zhang JH, editors. Animal Models of Acute Neurological Injuries II: Injury and Mechanistic Assessments, Volume 1. Totowa, NJ: Humana Press; 2012. p. 473-9.

Supplementary Table 1. Statistical methods and results.

Figure		n number: Control/Normal	n number: SAH	Test	Result	p-value
1a	Maximum NFL	19	42	unpaired T-test	t=8.504,df=59	<0.0001
1c	Normal vs High NFL	12	30	unpaired T-test	t=2.757,df=40	0.0087
1d	Ln Total Hb vs Ln predicted_NFL	N/A	42	Multivariable linear regression	B=0.364(0.156-0.573)	0.001

Figure		n number: Vehicle	Hb	Hb+Hp	Hp	Test		Result	p-value	Group comparisons: false discovery rate, Q=0.05: Vehicle vs Hb	Vehicle vs Hp	Hb vs Hb+Hp	Group comparisons: Bonferroni: Vehicle vs Hb	Vehicle vs Hp	Hb vs Hb+Hp	Group comparisons: other: Vehicle vs Hb	Vehicle vs Hp	Hb vs Hb+Hp
2c	*in vitro* Hb titration	5	5(all conditions)	N/A	N/A	One-way ANOVA		F(5,24)=17.89	<0.0001							0.001 (10µM, D1)		
2d	*in vitro* Hp efficacy	5	5	5	5	two-way ANOVA	interaction	F(1,16)=11.98	0.0032	0.003	ns	0.0016	0.0059	ns	0.0016			
3f	post-surgery ambulation	11	16	15	9	LMM	interaction	F(1,39.229)=4.136	0.049							0.003	ns	0.036
3g	post-surgery freezing	11	16	15	9	LMM	Interaction	F(1,45.621)=3.572	0.065							0.025	ns	0.041
4e	cortex Iba1+ IHC	13	11	10	7	two-way ANOVA	interaction	F(1,37)=10.13	0.003	0.0002	ns	0.0156	0.000198	ns	0.0312			
4i	SR+ Iba1+ IHC	11	11	10	7	two-way ANOVA	interaction	F(1,35)=1.364	0.2508									
							main effect_Hb	F(1,35)=4.455	0.042	0.0494	ns	0.0494	ns	ns	ns			
							main effect_Hp	F(1,35)=2.889	0.0981									
4m	SR+ GFAP+ IHC	13	11	9	8	two-way ANOVA	interaction	F(1,37)=5.376	0.026	0.0164	ns	0.0199	0.0164	ns	0.0397			
4q	hippocampal SY38 IHC	11	10	10	8	two-way ANOVA	interaction	F(1,35)=3.481	0.0705									
							main effect_Hb	F(1,35)=8.055	0.0075	0.0028	0.0018	0.0028	0.0084	0.0018	0.0066			
							main effect_Hp	F(1,35)=9.392	0.0042									
5a-d	CD163 IHC	8-13	10-12	9-10	7-8	Kruskal-Wallis			ns	ns	ns	ns				ns	ns	ns
5g	Perls' parenchyma	12	11	9	8	Kruskal-Wallis			0.0002	0.0004	ns	0.0385				0.0004(D2)	ns	ns
5h	Perls'convexity	13	12	9	8	Kruskal-Wallis			0.0003	0.0008	ns	ns				0.0011(D2)	ns	ns
6c	Ipsilateral MCA width	11	11	11	11	two-way ANOVA	interaction	F(1,40)=1.020	0.3186									
							main effect_Hb	F (1,40)=8.514	0.0058	0.0249	ns	ns	0.0498	ns	0.0128			
							main effect_Hp	F(1,40)=2.986	0.0917									
6d	Ipsilateral parenchymal SMA+ vessels	11	11	11	11	two-way ANOVA	interaction	F(1,40)=6.062	0.0182	0.0296	ns	0.0171	0.0593	ns	0.0171			
6e	Ipsilateral parenchymal Hb IHC	11	11	10	9	Kruskal-Wallis			0.0001	0.0249	ns	0.0013				ns	ns	0.0076(D2)
S2	Ambulation scores AUC	7	12	10	5	two-way ANOVA	interaction	F(1,30)=4.097	0.0519									
							main effect_Hb	F(1,30)=0.8865	0.3539	0.0206	ns	ns	0.0034	ns	0.0176			
							main effect_Hp	F (1,30)=4.589	0.0404									
S3a	total hippocampus Iba1+ cells	11	11	10	7	two-way ANOVA	interaction	F(1,36)=0.06971	0.7933									
							main effect_Hb	F(1,36)=2.872	0.098	ns	ns	ns	ns	ns	ns			
							main effect_Hp	F (1,36)=0.5818	0.4506									
S3b	total hippocampal GFAP+ cells	13	11	9	8	two-way ANOVA	interaction	F(1,37)=1.082	0.3051									
							main effect_Hb	F(1,37)=6.208	0.0173	0.0282	ns	0.0499	0.0564	ns	ns			
							main effect_Hp	F(1,37)=5.135	0.0294									
S3c	cortex GFAP+ cells	5	6	7	4	two-way ANOVA	interaction	F(1,17)=0.2886	0.5981									
							main effect_Hb	F(1,17)=0.02637	0.8729	ns	ns	ns	ns	ns	ns			
							main effect_Hp	F(1,17)=0.4274	0.522									
S4	PSD-95 immunoblot	4	4	4	4	two-way ANOVA	interaction	F(1,12)=3.689	0.0788									
							main effect_Hb	F(1,12)=13.92	0.0029	0.005	ns	0.005	0.0106	ns	0.0149			
							main effect_Hp	F(1,12)=12.02	0.0047									
Parenchyma	S5a	Perls vs cortical Iba1+ cells	13	11	9	7	weighted Pearson's r		0.9	0.05									
	S5b	Perls vs total hippocampal Iba1+ cells	11	12	9	8	weighted Pearson's r		0.976	0.012									
	S5c	Perls vs total hippocampal GFAP+ cells	13	11	8	8	weighted Pearson's r		0.934	0.033									
	S5d	Perls vs hippocampal SY38 IHC	11	10	9	8	weighted Pearson's r		-0.961	0.02									
	S5e	Perls vs AUC ambulation	7	12	9	5	weighted Pearson's r		-0.996	0.002									
	S5f	Perls vs AUC freezing	7	12	9	5	weighted Pearson's r		0.932	0.034									
Convexity	S5g	Perls vs cortical Iba1+ cells	12	10	9	7	weighted Pearson's r		0.898	0.051									
	S5h	Perls vs total hippocampal Iba1+ cells	11	11	9	8	weighted Pearson's r		0.939	0.031									
	S5i	Perls vs total hippocampal GFAP+ cells	12	10	8	8	weighted Pearson's r		0.956	0.022									
	S5j	Perls vs hippocampal SY38 IHC	10	9	9	8	weighted Pearson's r		-0.985	0.008									
	S5k	Perls vs AUC ambulation	7	11	9	5	weighted Pearson's r		-0.961	0.039									
	S5l	Perls vs AUC freezing	7	11	9	5	weighted Pearson's r		0.883	0.059									
	S6a	Ipsilateral ACA width	11	10	11	10	two-way ANOVA	main effect Hb	F(1,38)=3.444	0.0712	ns	ns	ns	ns	ns	ns			
	S6b	Contralateral ACA width	11	10	11	9	two-way ANOVA	main effect Hb	F(1,37)=8.319	0.0065	0.0618	ns	ns	ns	ns	ns			
	S6c	Contralateral MCA width	11	11	10	11	two-way ANOVA	main effect Hb	F(1,39)=6.440	0.0153	ns	ns	ns	ns	ns	ns			

Key:
D1=Dunnett's
D2=Dunn's
ns=non-significant
LMM=linear mixed modelling
significant test
significant p-value
marginal p-value

Note: in two-way ANOVAs, main effects (Hb and Hp) are only shown in the absence of an interaction (Hb x Hp) with p <0.05

Supplementary Figure 1

Free iron assay. Mouse Hb is stable following a two-week incubation at 37°C, with negligible release of free chelatable iron. 50µM mouse Hb ± an equimolar-binding ratio of Hp was incubated for 0, 7 and 14 days. After reduction to its ferrous state, free iron was analysed via reaction with the chelator TPTZ [2,4,6-Tri-(2-pyridyl)-5-triazine]; absorbance was measured at 600/800nm on an AU5800 Beckman Coulter analyser. n=6 experiments each with duplicate assays per condition, mean ±SEM.

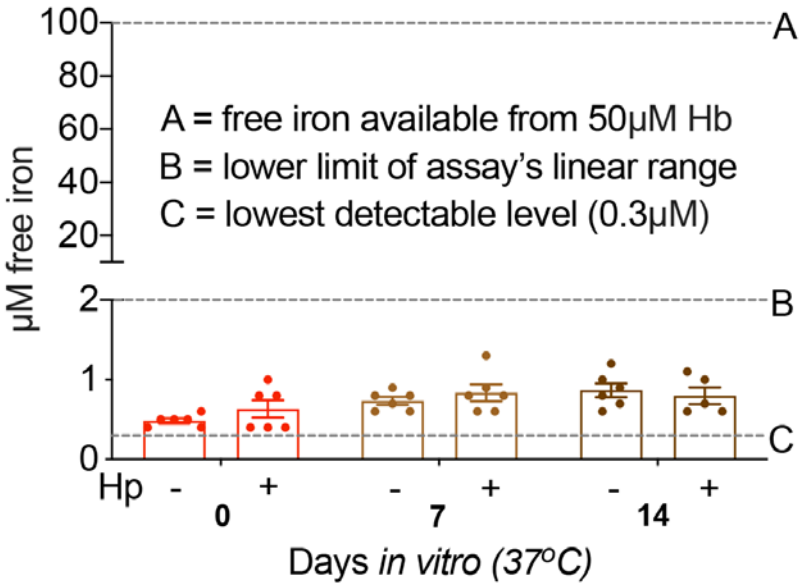

Supplementary Figure 2

Ambulation scores during laser-monitored open-field behavioural testing, not normalized to baseline (n=9-16 per condition). Mean area under the curve ±SEM. *p* values $*p < 0.05$, $**p < 0.01$.

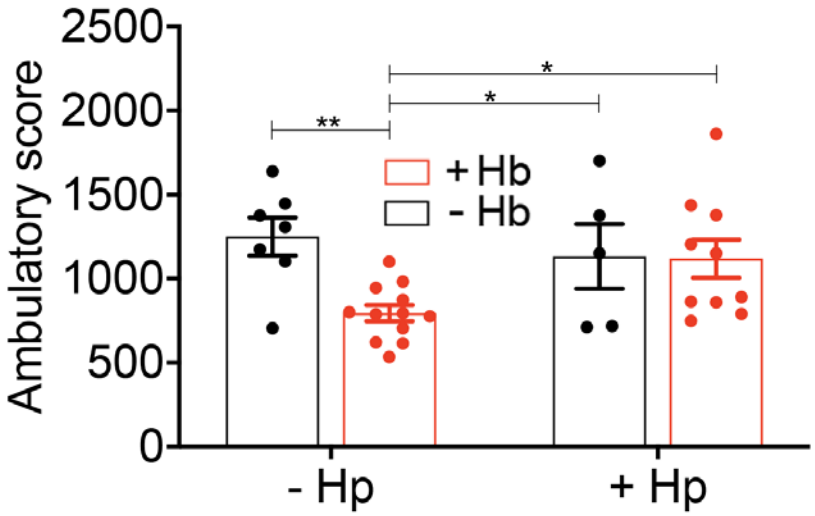

Supplementary Figure 3

Further Iba1 and GFAP immunohistochemistry. Quantification of total hippocampus lba1+ cell numbers ipsilateral to Hb infusion (**a,** n=7-11 per condition). Quantification of GFAP+ cell numbers ipsilateral to Hb infusion in total hippocampus (**b**, n=8-13 per condition) and cortex (**c**, n=7-10 per condition). Mean ±SEM. *p* values **p* < 0.05.

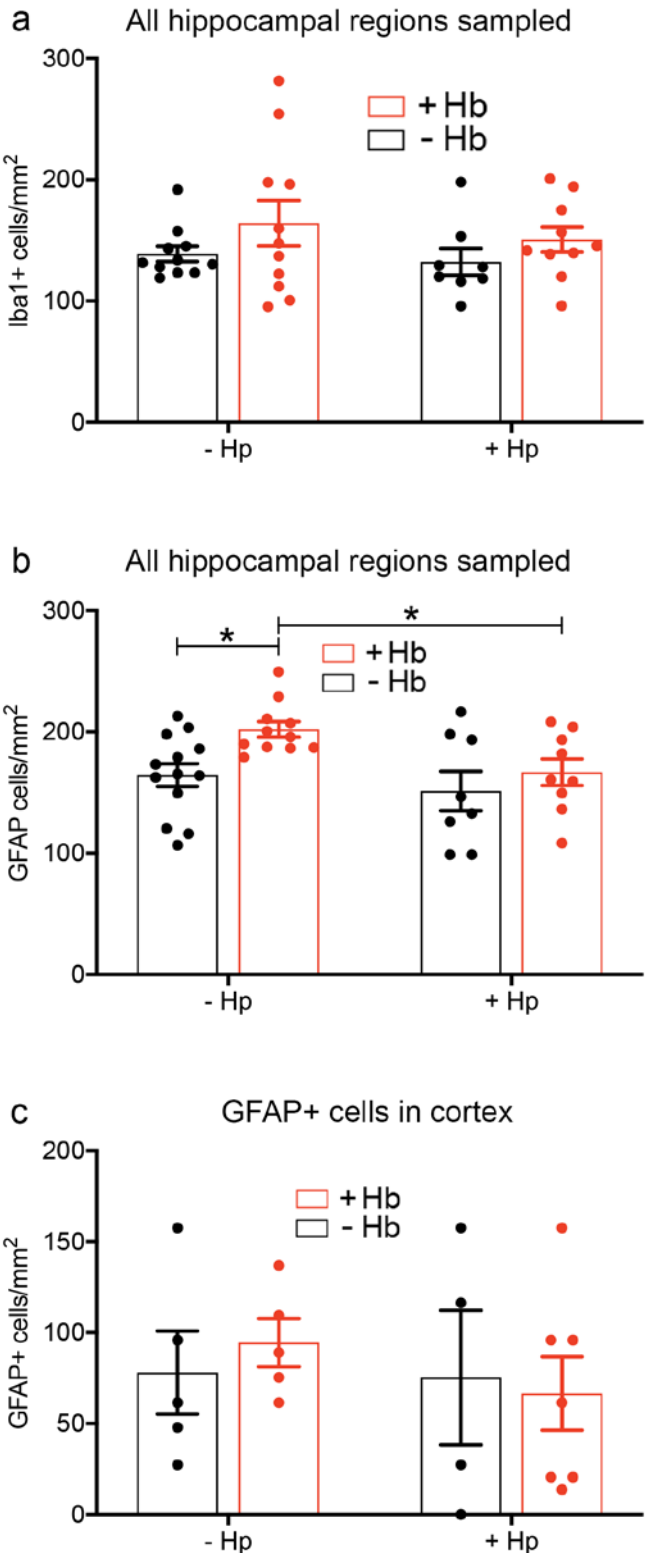

Supplementary Figure 4

PSD95 western blot. Immunoblot for postsynaptic density protein 95 (psd-95) in the hemisphere ipsilateral to Hb infusion (n=4 per condition, mean ±SEM). *p* values $^{**}p < 0.01$. Cropped and full length versions of a representative blot are shown.

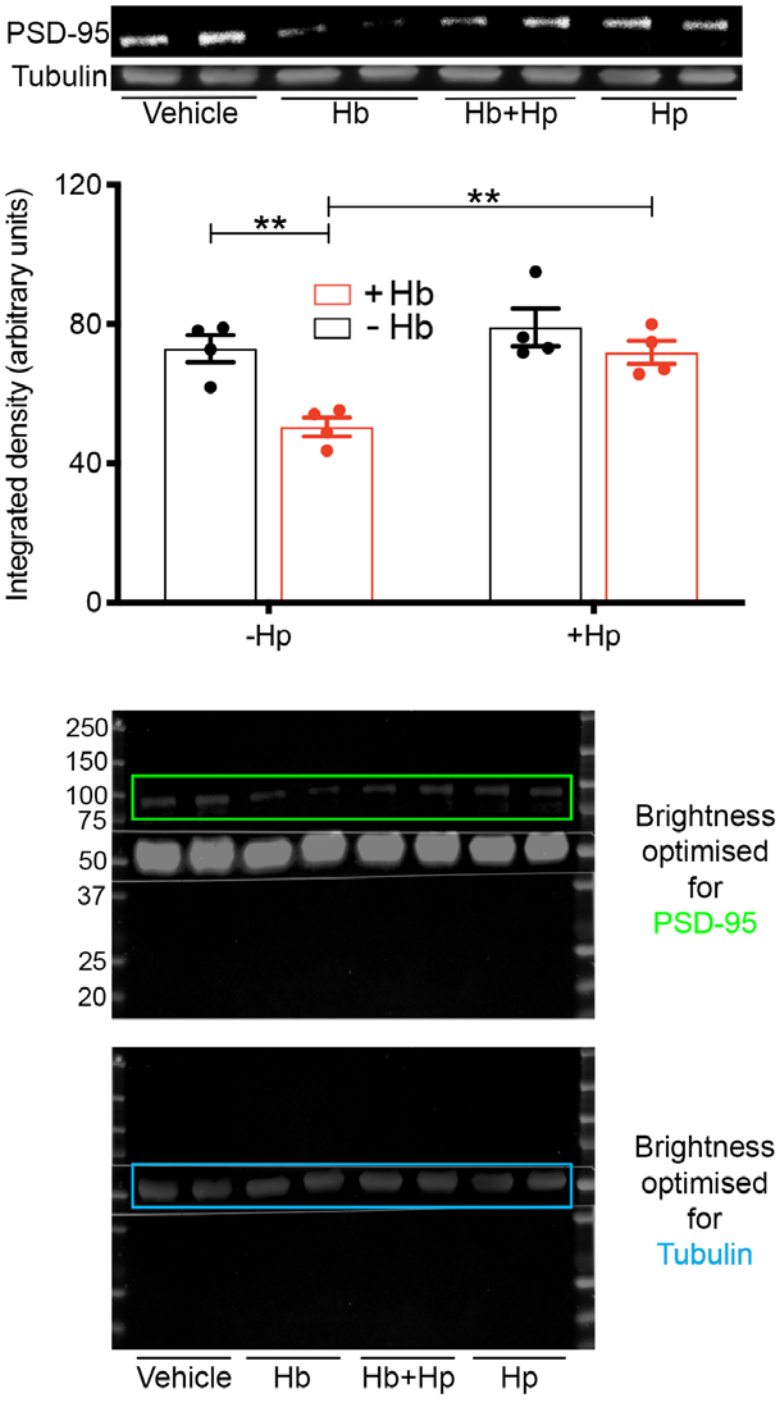

Supplementary Figure 5

Correlations of Perls' staining with pathology. Iron deposition is correlated with markers of inflammation, injury, synapse loss, and behavioural deficits. Animals are grouped by treatment representing high (Hb), low (vehicle & Hp), and intermediate (Hb+Hp) iron deposition. Weighted Pearson's correlations were calculated between Perls' staining (**a**,**b**,**c**,**d**,**e**,**f**, parenchyma; **g**,**h**,**i**,**j**,**k**,**l**, convexity) and immunohistochemical (n=7-13 per condition, mean ±SEM) and behavioural readouts (n=5-12 per condition, mean ±SEM). Perls' staining correlated positively with Iba1+ cells in the cortex (**a**,**g**), Iba1+ cells in the whole hippocampus (**b**,**h**), GFAP+ cells in the whole hippocampus (**c**,**i**), and freezing behaviour (**f**,**l**). Perls' staining correlated negatively with hippocampal Sy38 (**d**,**j**) and ambulation (**e**,**k**).

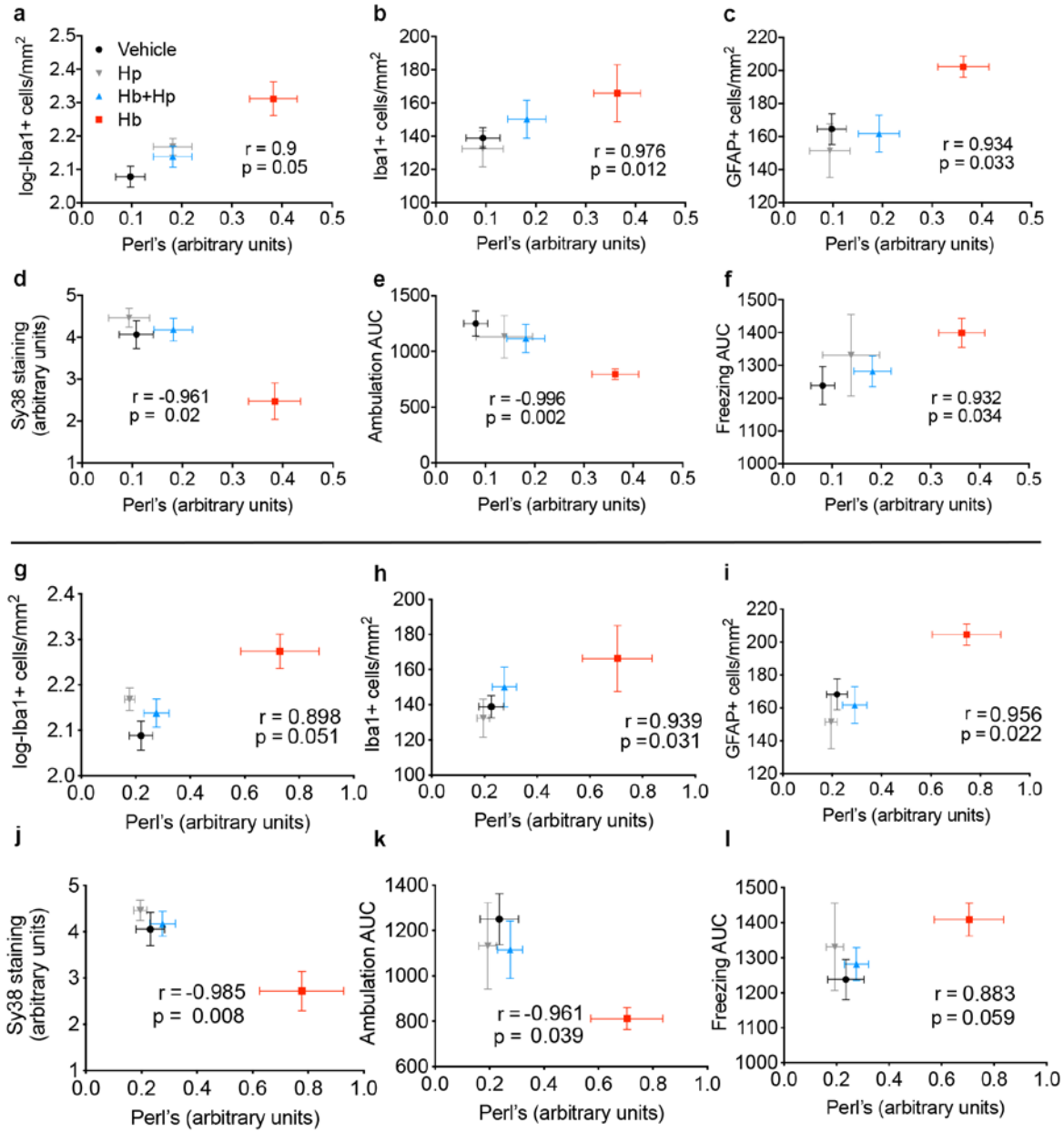

Supplementary Figure 6

Large cerebral artery vasospasm. Quantification of arterial diameter of cerebral arteries, other than the ipsilateral MCA. **a**, Ipsilateral anterior cerebral artery (ACA; n=10-11, two-way ANOVA: main effect Hb=0.0712, mean ±SEM). **b**, Contralateral ACA (n=9-11, two-way ANOVA: main effect Hb=0.0065, mean ±SEM). **c**, Contralateral MCA (n=10-11, two-way ANOVA: main effect Hb=0.0153, mean ±SEM). *p* value **p* < 0.05.

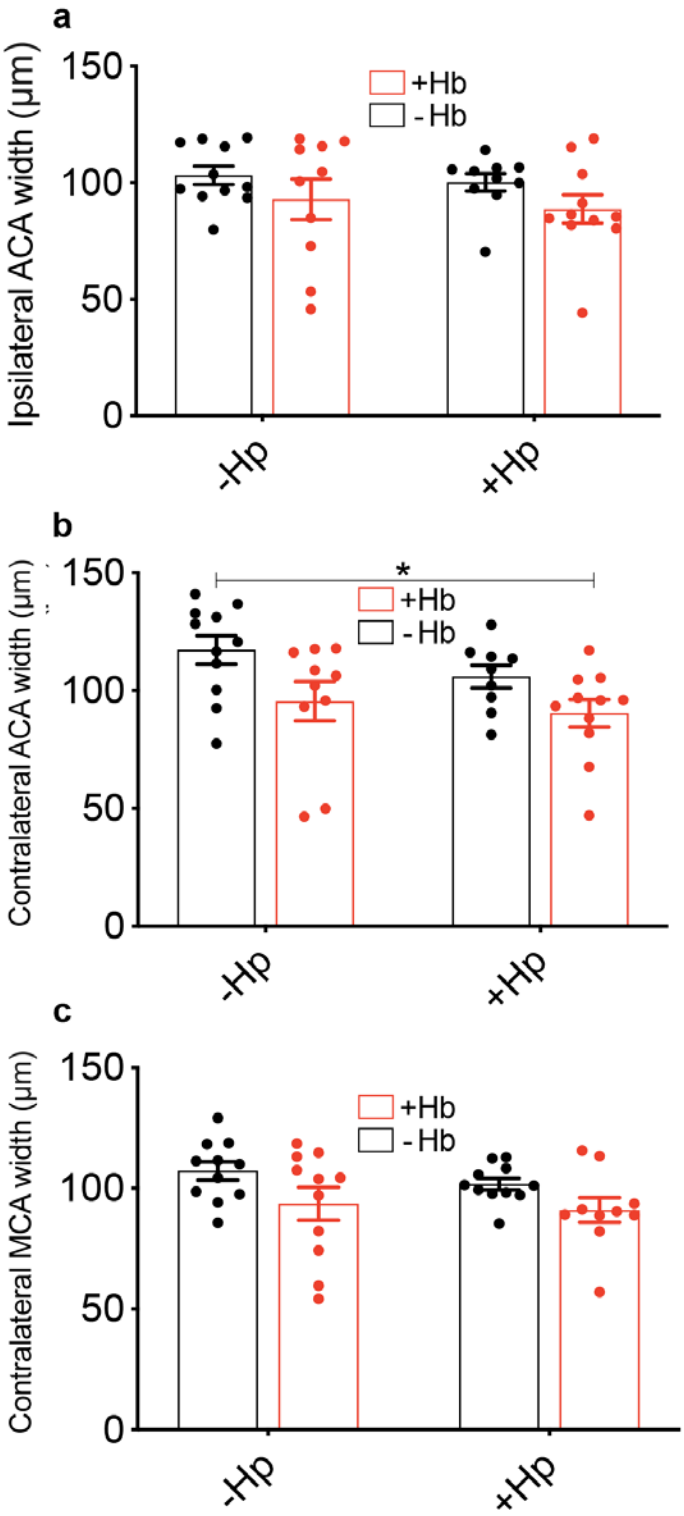

Supplementary Figure 7

Purity of mouse Hb preparation. SDS-PAGE of multiple Hb preparations demonstrates purity of Hb preparation. 10µg of total protein from seven individual Hb preparations were separated using reducing SDS-PAGE. Coomassie stain was used to identify protein bands. Only one protein (Hb) was visible.

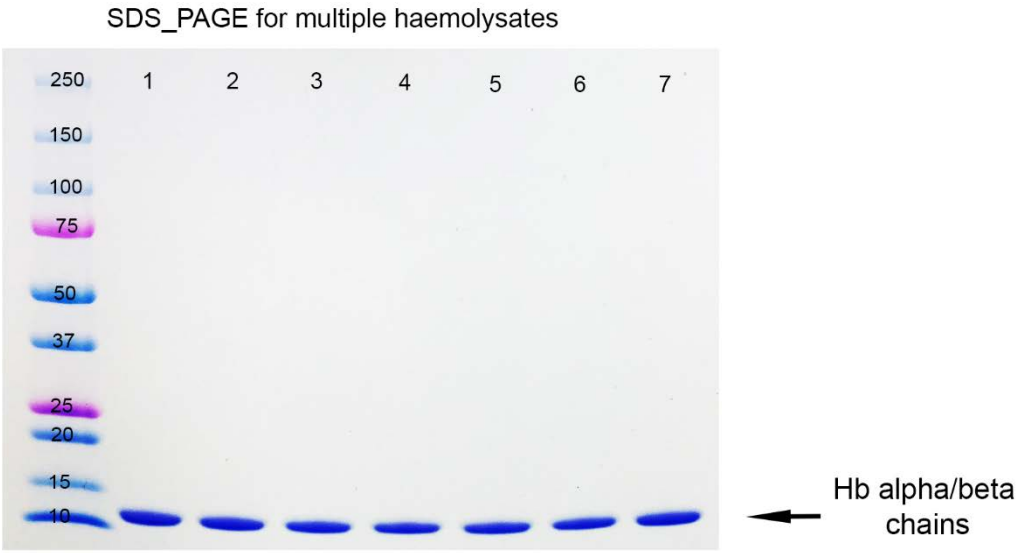

Supplementary Figure 8

Hb-Hp binding curve. Determination of Hb to Hp binding ratio. Increasing concentrations of mouse Hb were incubated with a fixed concentration of human Hp (1 mg/ml) and analysed using UPLC (see Methods). n=3, ±SEM. Saturated binding was observed at a 1:1.4 Hp to Hb ratio, identical to the binding ratio of the same batch of haptoglobin to human haemoglobin.

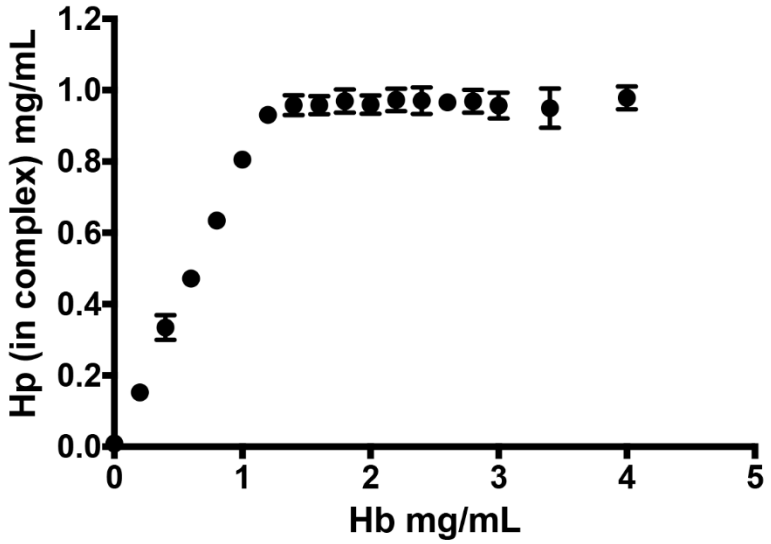

Supplementary Figure 9

Freezing score. Zonal analysis of open-field data. To assess acute freezing behaviour, the open-field arena was partitioned into inner and outer zones and the amount of time spent immobile in the outer zone recorded in the first minute.

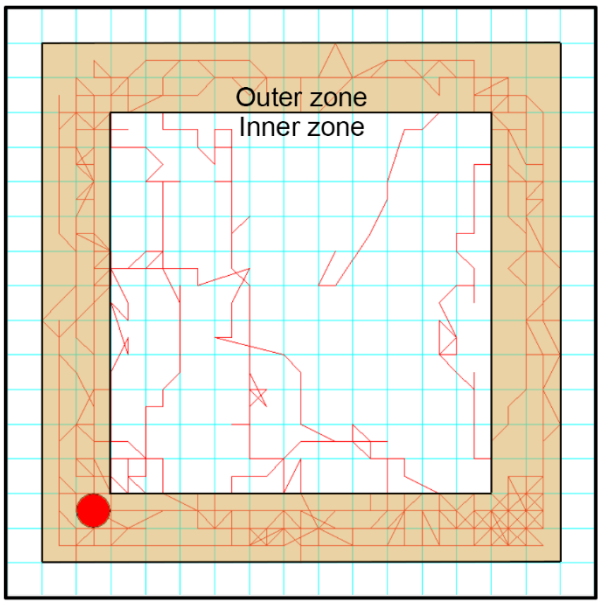

Supplementary Figure 10